The Astrophysical Journal, 939:6 (27pp), 2022 November 1 https://doi.org/10.3847/1538-4357/ac913b

The 2019 Outburst of the 2005 Classical Nova V1047 Cen: A Record Breaking Dwarf Nova Outburst or a New Phenomenon?

E. Aydi[1,30], K. V. Sokolovsky[1,2], J. S. Bright[3], E. Tremou[4], M. M. Nyamai[5], A. Evans[6], J. Strader[1], L. Chomiuk[1], G. Myers[7], F-J. Hambsch[8,9,10], K. L. Page[11], D. A. H. Buckley[5,12], C. E. Woodward[13], F. M. Walter[14], P. Mróz[15,16], P. J. Vallely[17], T. R. Geballe[18], D. P. K. Banerjee[19], R. D. Gehrz[13], R. P. Fender[3,5], M. Gromadzki[16], A. Kawash[1], C. Knigge[20], K. Mukai[21,22], U. Munari[23], M. Orio[24,25], V. A. R. M. Ribeiro[26,27], J. L. Sokoloski[28], S. Starrfield[29], A. Udalski[16], and P. A. Woudt[5]

[1] Center for Data Intensive and Time Domain Astronomy, Department of Physics and Astronomy, Michigan State University, East Lansing, MI 48824, USA
aydielia@msu.edu
[2] Sternberg Astronomical Institute, Moscow State University, Universitetskii pr. 13, 119992 Moscow, Russia
[3] Astrophysics, Department of Physics, University of Oxford, Keble Road, Oxford, OX1 3RH, UK
[4] National Radio Astronomy Observatory, P.O. Box O, Socorro, NM 87801, USA
[5] Department of Astronomy, University of Cape Town, Private Bag X3, Rondebosch 7701, South Africa
[6] Astrophysics Group, Keele University, Keele, Staffordshire, ST5 5BG, UK
[7] American Association of Variable Star Observers, 5 Inverness Way, Hillsborough, CA 94010, USA
[8] Vereniging Voor Sterrenkunde (VVS), Oostmeers 122 C, B-8000 Brugge, Belgium
[9] Groupe Européen d'Observations Stellaires (GEOS), 23 Parc de Levesville, F-28300 Bailleau l'Evêque, France
[10] Bundesdeutsche Arbeitsgemeinschaft für Veränderliche Sterne (BAV), Munsterdamm 90, D-12169 Berlin, Germany
[11] School of Physics & Astronomy, University of Leicester, LE1 7RH, UK
[12] South African Astronomical Observatory, P.O. Box 9, 7935 Observatory, South Africa
[13] Minnesota Institute for Astrophysics, School of Physics & Astronomy, 116 Church Street SE, University of Minnesota, Minneapolis, MN 55455, USA
[14] Department of Physics & Astronomy, Stony Brook University, Stony Brook, NY 11794-2100 USA
[15] Division of Physics, Mathematics, and Astronomy, California Institute of Technology, Pasadena, CA 91125, USA
[16] Astronomical Observatory, University of Warsaw, Al. Ujazdowskie 4, 00-478 Warszawa, Poland
[17] Department of Astronomy, The Ohio State University, 140 West 18th Avenue, Columbus, OH 43210, USA
[18] Gemini Observatory/NSF's NOIRLab, 670 N. Aóhoku Place Hilo, HI, 96720, USA
[19] Physical Research Laboratory, Navrangpura, Ahmedabad, Gujarat 380009, India
[20] School of Physics and Astronomy, University of Southampton, Highfield, Southampton, SO17 1BJ, UK
[21] CRESST II and X-ray Astrophysics Laboratory, NASA/GSFC, Greenbelt, MD 20771, USA
[22] Department of Physics, University of Maryland, Baltimore County, 1000 Hilltop Circle, Baltimore, MD 21250, USA
[23] INAF Astronomical Observatory of Padova, I-36012 Asiago (VI), Italy
[24] INAF–Osservatorio di Padova, vicolo dell'Osservatorio 5, I-35122 Padova, Italy
[25] Department of Astronomy, University of Wisconsin, 475 N. Charter Street, Madison, WI 53704, USA
[26] Instituto de Telecomunicações, Campus Universit ário de Santiago, 3810-193 Aveiro, Portugal
[27] Departamento de Física, Universidade de Aveiro, Campus Universitário de Santiago, 3810-193 Aveiro, Portugal
[28] Columbia Astrophysics Laboratory and Department of Physics, Columbia University, New York, NY 10027, USA
[29] School of Earth and Space Exploration, Arizona State University Tempe, AZ 85287-1404, USA
Received 2021 August 17; revised 2022 September 7; accepted 2022 September 10; published 2022 October 26

Abstract

We present a detailed study of the 2019 outburst of the cataclysmic variable V1047 Cen, which hosted a classical nova eruption in 2005. The peculiar outburst occurred 14 yr after the classical nova event and lasted for more than 400 days, reaching an amplitude of around 6 magnitudes in the optical. Early spectral follow-up revealed what could be a dwarf nova (accretion disk instability) outburst. However, the outburst duration, high-velocity (>2000 km s^{-1}) features in the optical line profiles, luminous optical emission, and presence of prominent long-lasting radio emission together suggest a phenomenon more exotic and energetic than a dwarf nova outburst. The outburst amplitude, radiated energy, and spectral evolution are also not consistent with a classical nova eruption. There are similarities between V1047 Cen's 2019 outburst and those of classical symbiotic stars, but pre-2005 images of the field of V1047 Cen indicate that the system likely hosts a dwarf companion, implying a typical cataclysmic variable system. Based on our multiwavelength observations, we suggest that the outburst may have started with a brightening of the disk due to enhanced mass transfer or disk instability, possibly leading to enhanced nuclear shell burning on the white dwarf, which was already experiencing some level of quasi-steady shell burning. This eventually led to the generation of a wind and/or bipolar, collimated outflows. The 2019 outburst of V1047 Cen appears to be unique, and nothing similar has been observed in a typical cataclysmic variable system before, hinting at a potentially new astrophysical phenomenon.

Unified Astronomy Thesaurus concepts: Classical novae (251); Dwarf novae (418); White dwarf stars (1799); Compact objects (288); Symbiotic binary stars (1674); Novae (1127)

[30] NHFP Hubble Fellow.

1. Introduction

Cataclysmic variables (CVs) are interacting binary systems, each consisting of a white dwarf (WD) accreting material from a Roche-lobe-filling companion. The material flowing from the

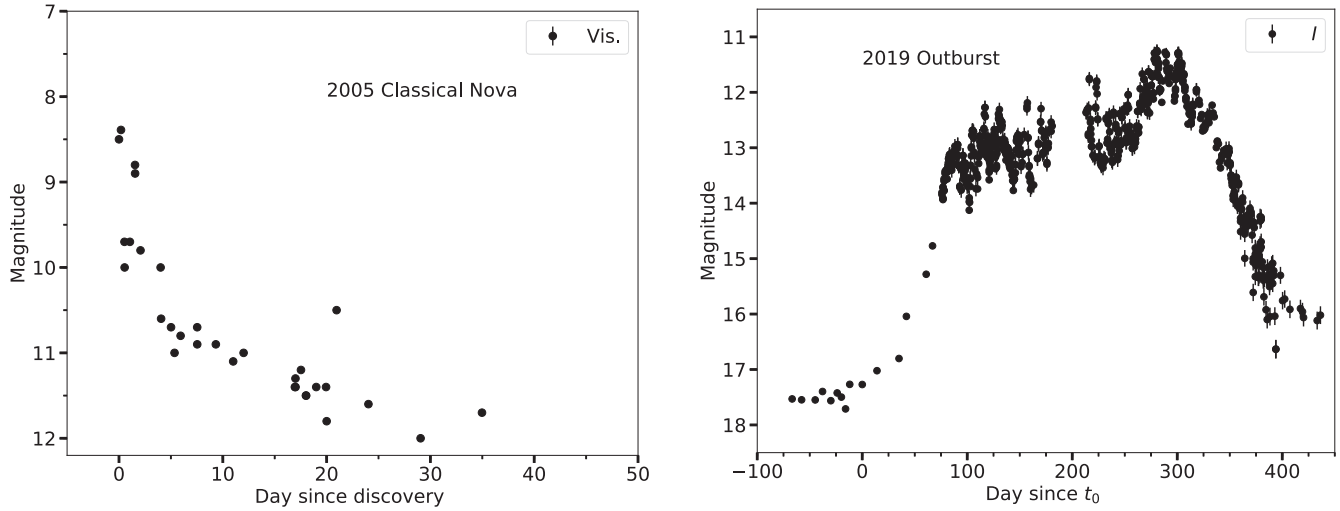

Figure 1. A direct comparison between the visual light curve of the 2005 classical nova eruption from AAVSO (*left*) and the OGLE *I*-band light curve of the 2019 outburst (*right*). The remarkable difference between the two light curves indicates that the two events are of a completely different nature.

companion forms an accretion disk around the WD before being dumped on its surface. In the case of a highly magnetized WD ($B > 10^6$ G), the magnetic field of the WD truncates the inner regions of the disk or even completely prevents it from being formed. In this case, the material follows the magnetic field lines onto the surface of the WD. These are known as magnetic CVs (see Warner 1995 for a review). CVs experience several types of cataclysmic events and thermonuclear explosions, hence the name. One of these events is called a dwarf nova (DN) and is a viscosity-induced instability in the accretion disk, resulting in a temporary increase in mass-transfer rate and heating the whole disk. DNe manifest as relatively low-amplitude outbursts, typically $\Delta m \sim 2$–5 mag up to ∼9–10 mag in some extreme cases (Kawash et al. 2021).

While material builds upon the surface of the WD through secular accretion, the pressure and density increase in its surface layers. Once a critical density is reached, a thermonuclear runaway is triggered on the surface of the WD, leading to an increase in the brightness of the system by up to 15 mag or more in a matter of a few days (Starrfield et al. 1972; Yaron et al. 2005). These events are known as classical novae (see Gallagher & Starrfield 1978; Bode & Evans 2008; Woudt & Ribiero 2014; Della Valle & Izzo 2020; Chomiuk et al. 2021a for reviews) and their recurrence timescale is typically ≳thousands of years (Yaron et al. 2005). In some cases, novae recur on shorter timescales—short enough to be recorded more than once. These are called recurrent novae and these systems are usually characterized by a high mass-transfer rate, often due to the presence of an evolved secondary (Schaefer 2010).

After a classical nova event, the mass-transfer rate is expected to be high enough to keep the disk in a hot, ionized state, temporarily preventing DNe in the system. Theoretically, DNe are only expected hundreds/thousands of years later, when the mass-transfer rate becomes low enough for the disk to cool and again become susceptible to disk instability events. This is implied by the hibernation scenario of CVs (Shara et al. 1986), which suggests that CVs go through cycles of low and high states of mass-transfer rate. In this scenario, the states are mostly determined by the irradiation of the secondary by a nova event (which increases the mass-transfer rate) and the growing separation between the two stars (which decreases the mass-transfer rate). However, several CV systems have shown DN outbursts after classical nova eruptions; e.g., GK Per (Sabbadin & Bianchini 1983; Bianchini et al. 1986; Zemko et al. 2017; Williams & Darnley 2018), V1017 Sgr (Sekiguchi 1992; Salazar et al. 2017), and V446 Her (Honeycutt et al. 1995, 2011; see Table A9 for a full list).

1.1. V1047 Cen—the 2019 Outburst

V1047 Cen (Nova Cen 2005) was discovered as a Galactic transient on 2005 September 1.03 at a visual magnitude of around 8.5 (left panel of Figure 1) and later classified spectroscopically as a classical nova eruption (Liller et al. 2005). Walter et al. (2012) reported spectroscopic follow-up taken approximately 5 and 7 days after discovery. The spectra showed typical lines of Balmer, Fe II, and O I, which are characteristic of a classical nova near the optical peak. The Balmer lines showed multiple P Cygni absorption components with blueshifted velocities of around 750 and 1800 km s^{-1}.

Otherwise, V1047 Cen was not extensively observed during the 2005 eruption, and little else is known about the classical nova eruption. Archival observations of the system, taken by the Inner Galactic Disk with MIPS (MIPSGAL; Carey et al. 2009) Survey in the 24 and 70 μm bands, yield a 24 μm average magnitude of 0.72 ± 0.02 mag (Gutermuth & Heyer 2015). The MIPSGAL survey data were collected between 2005 September and 2006 October. The system was also observed by the Wide-field Infrared Survey Explorer (WISE) on 2010 February with IR magnitudes $w1 = 11.2$, $w2 = 9.5$, $w3 = 4.2$, and $w4 = 2.2$. The high IR brightness early after the outburst could indicate a dust formation event, which is common among classical novae (see, e.g., Strope et al. 2010), as well as extinction along the line of sight. Additional archival observations by the VISTA Variables in the Via Lactea survey between 2010 March and 2011 August, show the nova fading from $K = 12.84$–13.11 (Saito et al. 2012). The Neil Gehrels Swift Observatory (hereafter Swift; Gehrels et al. 2004) observed the classical nova eruption between 2005 and 2008 (Ness et al. 2007). The observations obtained in 2005 November and 2006 January resulted in detections of hard X-rays from strongly absorbed shock emission, which are typically seen in novae during the early weeks/months of the eruption (see, e.g., Mukai et al. 2008; Schwarz et al. 2011;

Gordon et al. 2021). The Swift observations obtained in 2008 led to a non-detection in X-rays.

Fourteen years after the 2005 nova eruption, Delgado et al. (2019) reported the discovery of an astronomical transient AT2019hik/Gaia19cfn possibly associated with V1047 Cen on 2019 June 11.6, with a discovery magnitude of 16.2 in the G band. Based on regular monitoring by the Optical Gravitational Lensing Experiment (OGLE; Udalski et al. 2015) survey, Mroz & Udalski (2019) confirmed that the FK5 J2000 equatorial coordinates of the transient ($[\alpha, \delta] = [13^{h}20^{m}49\overset{s}{.}78, -62°37'50\overset{''}{.}6]$) were consistent with those of V1047 Cen. They found that the re-brightening of the system started as early as 2019 April 6.11 (HJD 2458579.61; right panel of Figure 1). This date is considered as the outburst start (t_0) throughout this paper. Mroz & Udalski (2019) noted that the slow re-brightening of the system was inconsistent with a recurrent nova eruption. The re-brightening of the system triggered follow-up observations across the electromagnetic spectrum. Aydi et al. (2019a) reported optical spectroscopy, which showed DN outburst spectral features superimposed on the spectral features of a classical nova nebula. Geballe et al. (2019) reported infrared spectroscopy of the then ongoing outburst, during its first 160 days, concluding that the event was possibly a DN outburst. However, upon further follow-up, the 2019 outburst of V1047 Cen seems to be a more exotic phenomenon.

Here, we report on the multiwavelength follow-up of the 2019 outburst of V1047 Cen spanning the spectrum from X-ray to radio. In Section 2, we present the observations and data reduction. In Section 3, we provide our results, while in Section 4 we offer a discussion about the nature of the event and its peculiar observational features. Our conclusions are given in Section 5.

2. Observations and Data Reduction

2.1. Optical and NIR Photometry

V1047 Cen has been observed by the OGLE sky survey (Udalski et al. 2015) since May 2013, several years before the outburst, as part of the OGLE Galaxy Variability Survey. All data were taken in the I band with an exposure time of 30 s, and they were reduced and calibrated using the standard OGLE pipeline (Udalski et al. 2015). A sample of the observations is listed in Table A1.

Optical photometry between days 76 and 437 was performed in the *BVRI* bands by several observers from the American Association of Variable Star Observers (AAVSO; Kafka 2020). The bulk of the multi-band photometry comes from two observers, Gordon Meyer and Josch Hambsch. A sample of the observations is listed in Table A2.

We obtained SMARTS *Andicam* photometry in the J, H, and K_s bands on 29 nights between days 80 and 117. Data reduction is described in Walter et al. (2012). A sample of the observations is listed in Table A3. The *Andicam* instrument was retired on 2019 August 1 (day 117). We also make use of IR photometry from the enhanced Wide-field Infrared Survey Explorer (NEOWISE; Mainzer et al. 2011) covering only three epochs during the outburst in the W1 (3.35 μm) and W2 (4.60 μm) bands. A log of the observations is listed in Table A4.

The field of V1047 Cen was observed by the Transiting Exoplanet Survey Satellite (TESS; Ricker et al. 2015) during sector 11, which covers the early rise of the 2019 outburst between days 17 and 44, and sector 38 covering the post-outburst period between days 753 and 781. We used the open-source tool ELEANOR (Feinstein et al. 2019) to extract light curves from the TESS full-frame images, opting to utilize the corrected flux light curve and to only include data that are not associated with a quality flag.

All the data will be available as online material. All multi-band photometry is calibrated using the *Vega* system zero-points.

2.2. Optical and IR Spectroscopy

We obtained optical and IR spectroscopic observations of the 2019 outburst between days 74 and 643 using a diverse group of telescopes and instruments. A log of the spectral observations is presented in Table A5.

We obtained spectra using the High Resolution Spectrograph (HRS; Barnes et al. 2008; Bramall et al. 2010, 2012; Crause et al. 2014) and the Robert Stobie Spectrograph (RSS; Burgh et al. 2003; Kobulnicky et al. 2003) mounted on the Southern African Large Telescope (SALT; Buckley et al. 2006; O'Donoghue et al. 2006) in Sutherland, South Africa. HRS was used in the low-resolution (LR) mode, yielding a resolving power $R = \lambda/\Delta\lambda \approx 14{,}000$ over the range of 4000–9000 Å. The primary reduction of the HRS spectroscopy was conducted using the SALT science pipeline (Crawford et al. 2010), which includes over-scan correction, bias subtraction, and gain correction. The rest of the reduction was done using the MIDAS FEROS (Stahl et al. 1999) and *echelle* (Ballester 1992) packages. The reduction procedure is described by Kniazev et al. (2016). RSS was used in long-slit mode with the 1.5′ slit and the PG900 grating, resulting in a resolving power $R \approx 1500$. The spectra were first reduced using the PySALT pipeline (Crawford et al. 2010), which involves bias subtraction, crosstalk correction, scattered light removal, bad pixel masking, and flat fielding. The wavelength calibration, background subtraction, and spectral extraction were done using the Image Reduction and Analysis Facility (IRAF; Tody 1986).

We also carried out low- and medium-resolution optical spectroscopy using the Goodman spectrograph (Clemens et al. 2004) on board the 4.1 m Southern Astrophysical Research (SOAR) telescope located on Cerro Pachón, Chile. The observations were carried out in two setups: one setup using the 400 l mm^{-1} grating and a 0.″95 slit, yielding a resolving power $R \approx 1000$ over the wavelength range of 3820–7850 Å. Another setup was used with a 2100 l mm^{-1} grating and a 0.″95 slit, yielding a resolving power $R \approx 5000$ in a region centered on Hα that is 570 Å wide. The spectra were reduced and optimally extracted using the APALL package in IRAF.

Four high-resolution spectra were also obtained using the Chiron fiber-fed echelle spectrograph (Tokovinin et al. 2013) mounted on the CTIO 1.5 m telescope. Integration times were 20 minutes, with three integrations per night summed for 1 hr net exposure time. All spectra were taken in *fiber mode*, with 4×4 on-chip binning yielding a resolving power $R \approx 27,800$. The data were reduced using a pipeline coded in IDL (Walter 2017).[31]

2.3. Infrared Spectroscopy

Near-infrared (NIR) spectra of V1047 Cen were obtained at the Gemini South Telescope on Cerro Pachon in Chile on days

[31] http://www.astro.sunysb.edu/fwalter/SMARTS/CHIRON/ch_reduce.pdf

223 and 230 using the facility instrument FLAMINGOS-2, for program GS-2020A-Q-201. The observations are summarized in Table A6. The 0.36″ wide slit and R3000 grism were employed to obtain spectra at resolving powers, R, of up to 3000 in portions of the J, H, and K windows. The JH R1200 grism was used with the same slit to obtain a spectrum covering 0.89–1.75 μm. Note that for each grism there is considerable variation in R across each wavelength interval. (see Ref.[32]). Data reduction employed standard NIR techniques utilizing both Gemini/IRAF and Figaro commands (Shortridge et al. 1992). Flux calibrations, derived from spectra of the standard stars listed in Table A6 and are accurate to $\pm$ 30%.

NASA SOFIA (Stratospheric Observatory for Infrared Astronomy; Young et al. 2012) airborne observations of V1047 Cen were obtained with the Faint Object InfraRed CAmera (Herter et al. 2018), the dual-channel mid-infrared imager and grism spectrometer operating from 5–40 μm on two separate, consecutive flight series on 2019 July 02.542 UT (F0589) 03.559 UT (F0590), days 88 and 89, using the G111 and G227 grisms with the instrument configured using a long-slit (4.″7 × 191″), yielding a spectral resolving power $R \sim 140$–300. the G111 grating was used to observe V1047 Cen both nights. Standard pipeline processed and flux calibrated data (for details of the reduction processes see Clarke et al. 2015) were retrieved for science analysis from the Infrared Processing and Analysis Center (IPAC) Infrared Science Archives (IRSA). The data products contain a computed atmospheric transmission model appropriate for the flight altitudes, which were used to mask out spectral points in the observed spectral energy distributions (SEDs) where the atmospheric transmission was $\lesssim$70%. Within the statistical errors, no variations between the G111 data sets obtained on the two different nights were noted; hence, these data were averaged into a single resultant spectrum.

2.4. MeerKAT Observations

We observed the field of V1047 Cen with the MeerKAT radio interferometer (Jonas & MeerKAT Team 2016) 15 times between days 277 and 700. Observations were taken with the 64 antenna array at a central frequency of 1.28 GHz with an 856 MHz bandwidth. Each observation consisted of 15 minutes of integration on the field of V1047 Cen with 2 minutes on the phase calibrator J1424-4913 before and after. J1939-6342 was used to set the flux scale and calibrate the bandpass response of the instrument. Data were reduced using the OxKAT (see Heywood 2020 for details) reduction scripts, which include recipes for both phase reference and amplitude and phase self-calibration. The typical noise in a region of our images without obvious emission is 35 μJy beam^{-1}. A log of the MeerKAT observations is given in Table A7

2.5. Swift Observations

Observations of V1047 Cen with Swift commenced on 2019 June 24, 79 days after the start of the re-brightening. The UV/Optical Telescope (UVOT; Roming et al. 2005) detected emission across all three UV filters (*uvw1*: central wavelength of 2600 Å; *uvm2*: 2246 Å; *uvw2*: 1928 Å; a sample of the observations is listed in Table A8). No X-ray emission was detected with the X-ray Telescope (XRT; Burrows et al. 2005), however. A second observation was performed a month later (day 109), followed by approximately weekly observations from day 123 until day 420 after the start of the outburst. Throughout this time, a variable UV source was detected, while no individual observations showed significant X-ray emission. Co-adding the full ∼50 ks of XRT data, a faint X-ray source with a count rate of $2.8^{+1.3}_{-1.1} \times 10^{-4}$ count s^{-1} was detected. However, with only 16 counts in the source extraction region, no spectral analysis can be sensibly performed.

[32] http://www.gemini.edu/instrumentation/flamingos-2/components#Grisms

3. Results

3.1. Optical/UV Light Curves

The AAVSO (*BVRI*), OGLE I, and Swift UV light curves of V1047 Cen are presented in Figure 2. The data reveal peculiar behavior, with the outburst lasting for around 400 days. There is a general trend of increased brightness between days 0 and ∼310, before the brightness of the system starts decreasing. Throughout the 400 day outburst, the light curves show variability on timescales of a few days and with an amplitude of $\lesssim$1 magnitude. Based on the OGLE data the amplitude of the outburst reached 6.2 magnitudes (Figure 1).

The evolution of the optical broadband colors $(B-V)_0$, $(V-R)_0$, and $(R-I)_0$ is presented in Figure 3. We applied a reddening correction based on the $E(B-V)$ extinction derived in Section 4.1. The colors show random fluctuations around a mean value throughout the majority of the outburst. However, on day 250, the three colors show a noticeable redward trend, coincident with a bump in the optical light curves. This is followed by a blueward trend after day 300, as the outburst ends.

We have NIR photometry only for a short period near the start of the plateau. Aside from a trend toward redder colors as the source brightened (between days 76 and 82, corresponding to the late part of the rising phase), the NIR colors were fairly stable, at $I-K = 2.25 \pm 0.03$, $J-K = 1.24 \pm 0.02$, and $H-K = 0.51 \pm 0.03$. We use our data to create multiwavelength SED of V1047 Cen during the 2019 outburst. Despite our extensive coverage of the outburst, we do not have simultaneous optical, IR, UV, and radio data except for one day (day ≈308), where we have simultaneous optical, UV, and NEOWISE NIR photometry, along with MeerKAT radio data (see Figure 4). Since the brightness of the system shows variability, up to 1 mag in a couple of days, we avoid any interpolation of the light curve to create SEDs on other days. We attempted a blackbody fit to the multiwavelength SED, but no blackbody model can result in a reasonable fit to the data and we end up with poor fitting even in the case of multiple blackbody components. This indicates complex emission, possibly from multiple sources (e.g., the nebula of the 2005 nova event, the WD surface, the accretion disk, and ejected material/outflow during the 2019 outburst). Similarly, we attempted a disk model fitting to the multiwavelength SED, but no disk model with reasonable parameters (e.g., mass accretion rate and disk radius) could fit the data, particularly due to the high brightness of V1047 Cen during outburst relative to accreting WD systems. Whether we include the MeerKAT data or not, the mass accretion rate resulting from the best-fit disk model to the SED is of the order of $10^{-5}\ M_\odot$ yr^{-1}, which is not physically reasonable. This shows that accretion alone is not enough to explain the emission during the outburst, again raising questions about its nature.

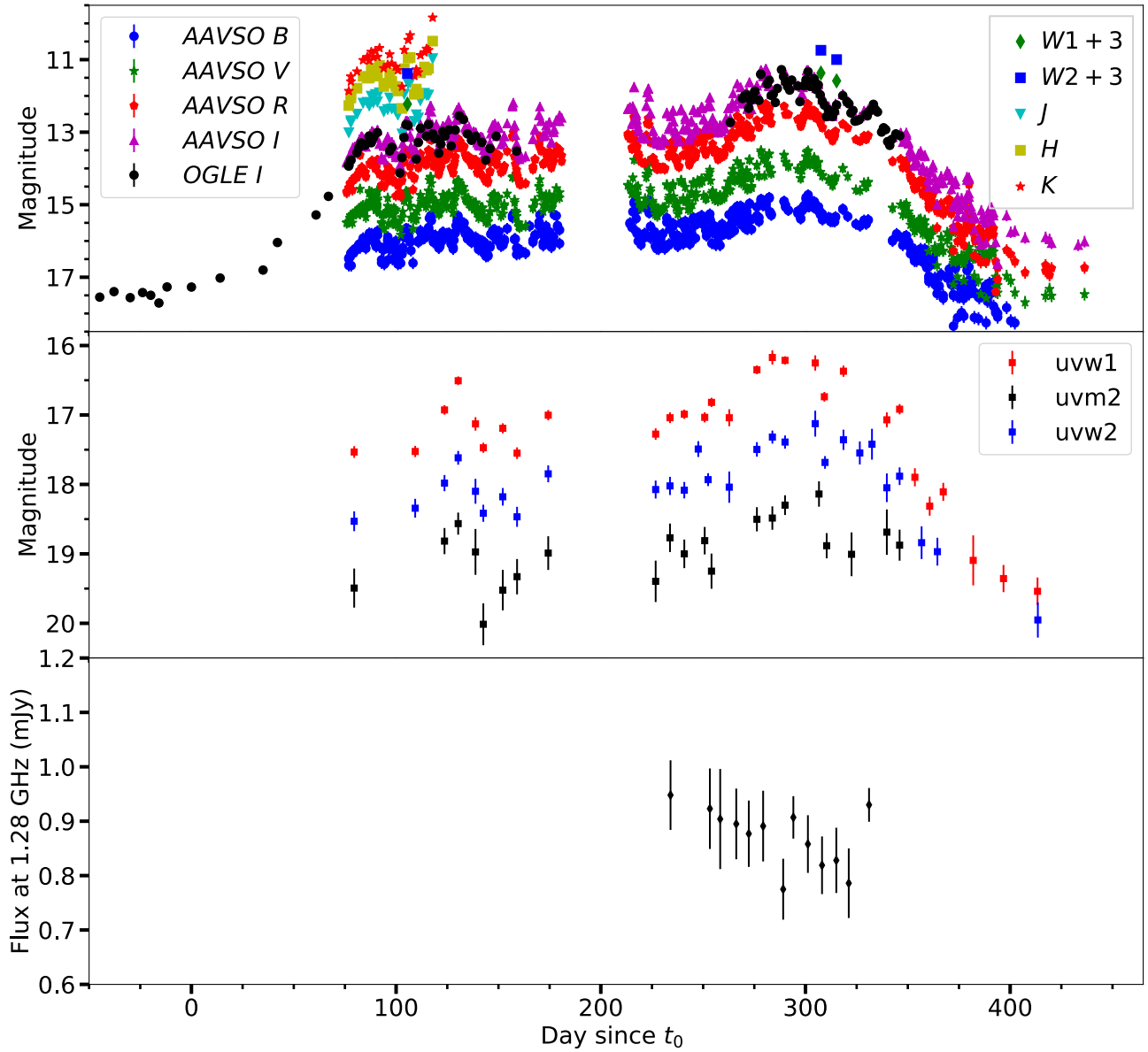

Figure 2. Multi-band light curves of the 2019 outburst of V1047 Cen. The *top panel* shows optical and IR photometry from AAVSO (*BVRI*), OGLE (*I*), SMARTS (*JHK*), and NEOWISE (W1 and W2) photometry. The *middle panel* shows Swift UVOT UV data, and the *bottom panel* shows MeerKAT *L*-band radio flux at 1.28 GHz. Colors and symbols are coded as indicated in figure legends.

The sector 11 TESS light curve of V1047 Cen, presented in Figure 5 (left panel), shows the early rise of the outburst between days 17 and 44. Aydi et al. (2019b) reported a period of 0.36 day in the TESS light curve. However, after extracting the data using different techniques and performing period analysis on the different light curves, we failed to find the period in some of these light curves. This indicates that the 0.36 day period is possibly an artifact introduced by the extraction technique or it is caused by emission leaking into the aperture from background, unresolved sources. This period is also not present in the TESS data from sector 38 (Figure 5, right panel), which covers the post-outburst period between days 753 and 781.

3.2. Radio Light Curve and Spectral Indices

The MeerKAT radio light curve is plotted in Figure 2. The *L*-band (900–1670 MHz) flux shows variability between ∼0.7 and 1.0 mJy during the optical outburst. There is no obvious correlation between the optical and radio emission. At day 700, 10 months after the end of the optical outburst, the radio emission from the system is still bright at 0.91 mJy (Figure 6).

We derived the spectral indices of the MeerKAT observations on days 258, 301, and 421 (Figure 6). To do that, we divided the data into eight frequency intervals centered at 859 MHz, 1.016 GHz, 1.123 GHz, 1.230 GHz, 1.337 GHz, 1.444 GHz, 1.551 GHz, and 1.658 GHz, allowing us to measure the flux density of the source at each sub-band. Consequently, we calculated the spectral index, α, by fitting a single power law to the radio spectra that is represented as: $S \propto \nu^{\alpha}$. We note that the sub-band calibration for MeerKAT is still an active area of exploration, and hence the systematic uncertainties on the sub-band flux densities may yet be underestimated. While the spectrum is mostly flat, given the large uncertainties in the spectral indices, caution is required when interpreting these indices. Overall, it is hard to draw

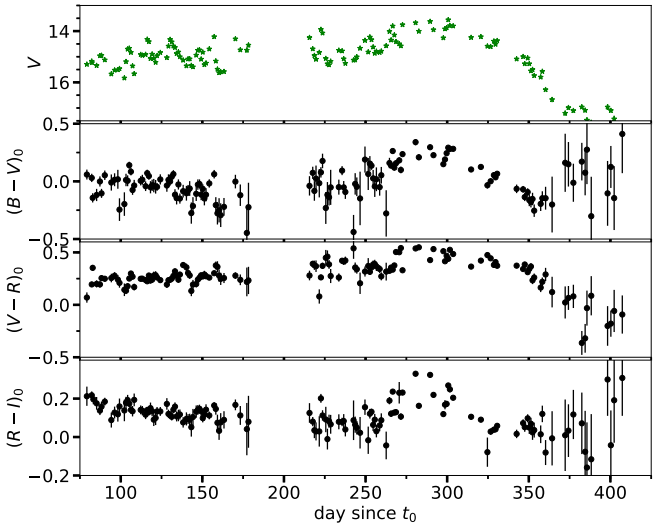

Figure 3. Evolution of the extinction-corrected broadband colors $(B-V)_0$, $(V-R)_0$, and $(R-I)_0$, throughout the outburst.

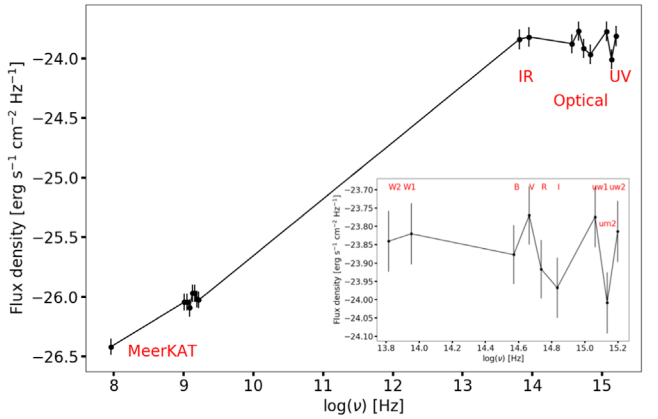

Figure 4. Extinction-corrected SED plot, showing the UV to radio SED of V1047 Cen on day 308. The error bars are 1σ uncertainties and they include contributions from the photometric and extinction uncertainties. We also present a zoom-in on the IR/optical/UV data.

strong conclusions from these values, other than that the radio emission is not optically thick. We elaborate more on the origin of the radio emission in Section 4.

3.3. Optical Spectral Evolution

In Figure 7 we present a sample of the optical spectra, evolving throughout the outburst of V1047 Cen and covering three stages: the rise (day 74), plateau phase (days 113 and 303), and post-outburst (day 407). The full spectral evolution is presented in Figures A1–A7. The first spectrum, obtained 74 days after the start of the outburst, shows relatively narrow emission lines of H (Balmer), He I, and He II, with FWHMs $<300\,\mathrm{km\,s^{-1}}$ and full widths at zero intensity (FWZIs) of around $500\,\mathrm{km\,s^{-1}}$, which are typical features of a DN outburst (e.g., Morales-Rueda & Marsh 2002) and low for classical nova eruptions. These features coexist and are superimposed on top of broader emission lines of H, O III, and C VI, with FWZIs of around $2500\,\mathrm{km\,s^{-1}}$ for the Balmer lines and $1100\,\mathrm{km\,s^{-1}}$ for the O III lines, which are characteristic of a classical nova nebula (likely arising in the remnant of the 2005 nova eruption). We also identify an even narrower feature in the Balmer lines, during the first two spectral epochs (days 74 and 81), characterized by FWHMs of $<40\,\mathrm{km\,s^{-1}}$ (see Figures 8 and A8). We do not have a definite explanation for the origin of these narrow features.

By day 113, the fluxes of the Balmer lines had increased significantly relative to the O III lines; compare $F_{\mathrm{H}\alpha}/F_{5007} = 1.56$ on day 74 with ∼15 on day 113 (e.g., $F_{\mathrm{H}\beta}/F_{5007}$ increased from ∼0.35 on day 74 to ∼3.1 on day 113; see Figure 9 for a direct comparison between the evolution of Hβ and the O III lines). The high-resolution spectra show that the Balmer and O III line profiles are very different from one another, with the O III lines (in the high-resolution spectra) having rectangular shapes and jagged tops, characteristic of nova nebular lines. In contrast, Hβ shows complex profiles which vary throughout the outburst. The Balmer lines also had significantly broadened from day 113, with the FWZIs increasing by a factor of ∼2 compared to day 74, reaching 4000–4500 $\mathrm{km\,s^{-1}}$ (Figures 8 and 9). Note that a broad base in Hα can be observed as early as day 81 but it becomes prominent from day 113 onward.

From day 130, some of the He I emission lines show P Cygni profiles with absorption troughs at blueshifted velocities of around $1400\,\mathrm{km\,s^{-1}}$ (Figures A2 and A3).

Between days 262 and 303 O I and N II emission lines emerge, while the O III nebular lines fade relative to the other spectral lines. At this stage, in addition to the He I emission lines, Balmer, N II and O I emission lines also show P Cygni profiles with absorption troughs at velocities of around -1200 to $-1400\,\mathrm{km\,s^{-1}}$ (Figure 10). During the same period, particularly on days 281 and 286, the optical spectra that extend above 8000 Å show broad double-peaked emission of O I at 8446 Å with FWZIs of around $3600\,\mathrm{km\,s^{-1}}$ (Figure A7). The O I P Cygni profile at 7773 Å and the double-peaked O I 8446 Å are not typical features of DN outbursts (Morales-Rueda & Marsh 2002).

After the end of the optical outburst, the spectrum obtained on day 407 shows substantial changes (Figure 7), with the O III emission lines now dominating the spectrum relative to the Balmer lines. In Figure 11 we show the evolution of the line ratio between the O III line at 5007 Å and Hβ and the evolution of the equivalent width (EW) of Hβ, O III 5007 Å, and O III 4995 Å emission lines. It is remarkable how the O III lines were still relatively strong during the rise of the 2019 outburst, but fade throughout the outburst, before strengthening again relative to the Balmer lines by the end of the outburst.

Half a year later, our spectra on days 615 and 643 still show strong O III lines, in addition to other lines, which likely originate in the 2005 classical nova nebula, such as O II 7320 Å, N II 5755 Å, and high ionization Fe VII lines (Figure A5).

Our last spectrum taken on day 774, more than 2 yr after the start of the 2019 outburst, shows in addition to the 2005 nova nebular lines, weak lines from high ionization transitions of He, N, O, and C, such as the He II lines at 4686 and 5412 Å, N V 4603 Å, O V 5920 Å, C IV 5802 Å, and O IV 7713 Å or Ne IV 7716 Å (Figure A6). Such lines have been observed in systems like V617 Sgr and V Sge, and are associated with nuclear shell burning (e.g., Herbig et al. 1965; Cieslinski et al. 1999; Steiner et al. 1999).

Several months after the end of the optical outburst on days 615 and 643, Hα shows satellite emission components at $\pm 2500\,\mathrm{km\,s^{-1}}$ (Figures 12 and A5). We elaborate on the origin of these components in the discussion.

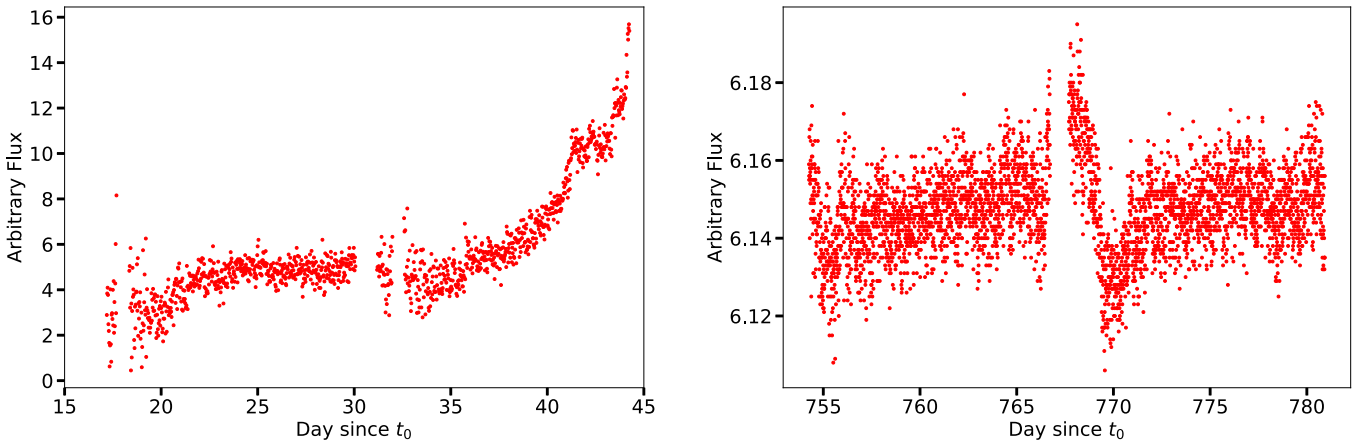

Figure 5. TESS light curve of the 2019 outburst of V1047 Cen during sectors 11 (*left*) and 28 (*right*).

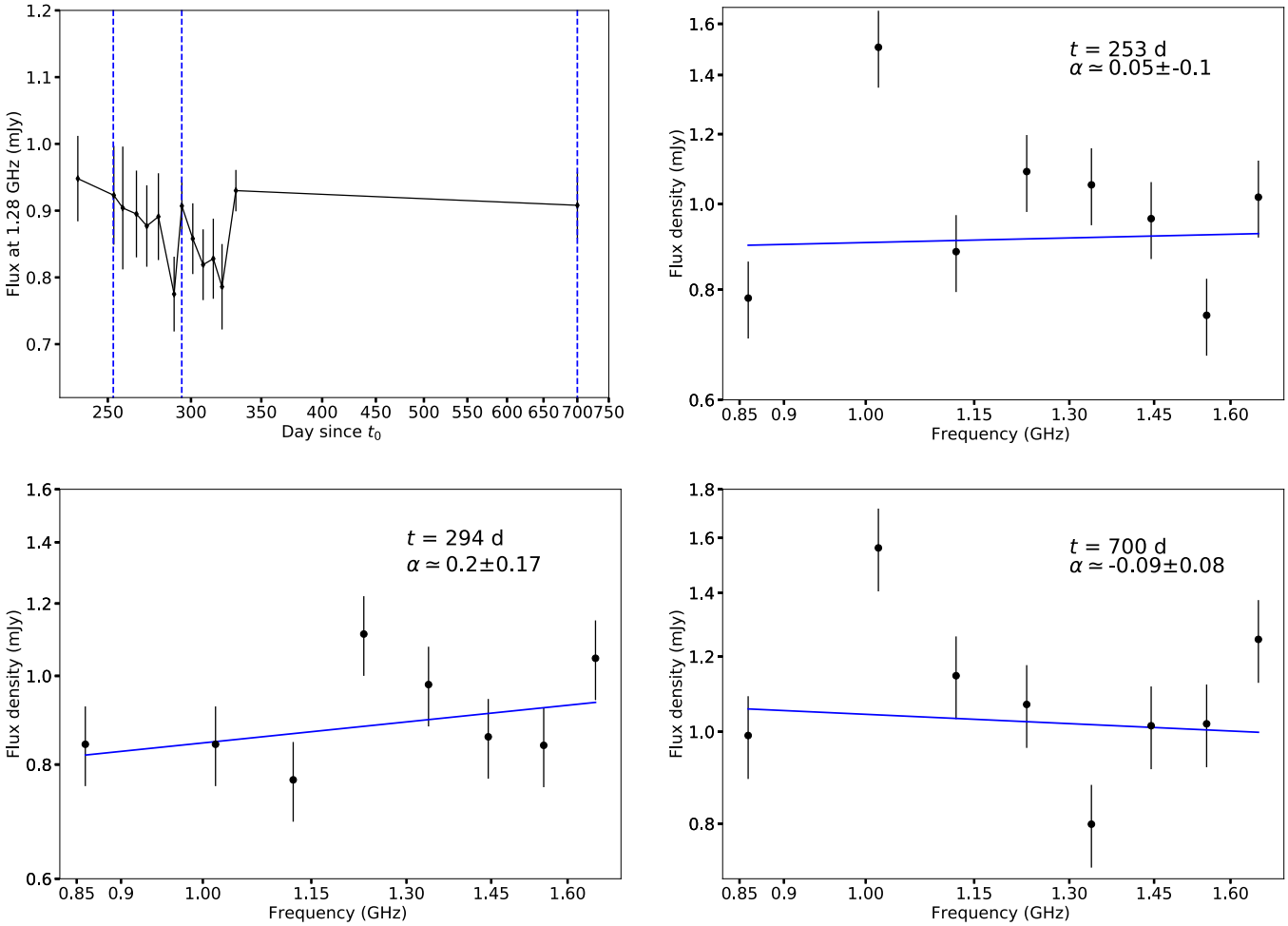

Figure 6. MeerKAT radio light curve measured at 1.28 GHz is plotted in the *top-left panel*, for comparison with three radio spectra measured on days 256, 294, and 700. Spectral indices are listed in each panel. The vertical dashed lines on the light-curve plot signify the epochs when spectra are measured.

3.4. IR Spectral Evolution

The Gemini and SOFIA IR spectra are represented in Figures 13 and 14, respectively. A detailed description and analysis of the IR spectral evolution during the first 120 days of the outburst is presented in Geballe et al. (2019). The Gemini *JHK* spectra obtained on day 323 show emission lines of H I (Paschen, Brackett, and Pfund series), He I, He II, and O I. The FWZIs of the lines are around 4000 km s^{-1}, similar to the ones measured from the optical spectral lines. The O I line at 1.1289 μm and some of the H I and He I lines show P Cygni profiles with absorption troughs at blueshifted velocities of 1100–1800 km s^{-1}, also comparable to the ones measured for optical lines (Figure 10).

Figure 14 presents the SOFIA composite spectra obtained on day 87, including contemporaneous, dereddened (see

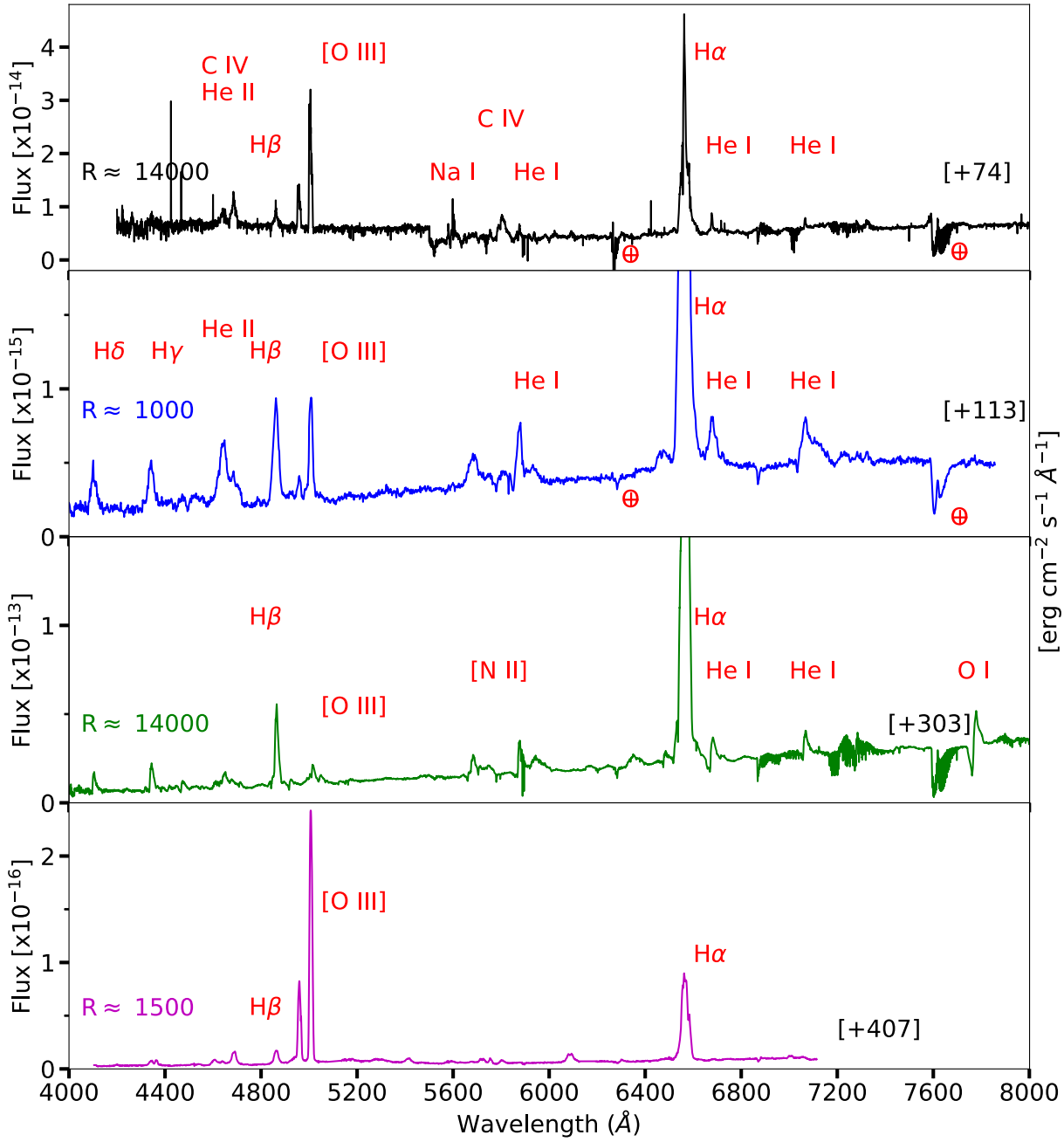

Figure 7. Optical spectral evolution of V1047 Cen throughout different stages of its outburst. The numbers in brackets are days since t_0. We also quote the resolving power of the spectra on the plot. Note that the calibration pipeline introduced artifacts in the continuum of the spectrum of day 74, particularly below 5000 Å.

Section 4.1) *BVRI* photometry obtained from the AAVSO database, as well as NEOWISE photometry obtained 18 days later. A blackbody fit to the 2019 SOFIA spectra yields $T_{\rm bb} = 425 \pm 12$ K, which we interpret as thermal emission from circumstellar material heated by the outburst event. WISE photometry obtained in 2010 (prior to the eruption) is also plotted and a blackbody fit to this photometry yields a cooler temperature of $T_{\rm bb} = 315 \pm 30$ K. Thus, the circumstellar material (dust, likely from the 2005 nova event) has been heated as a result of processes related to the 2019 outburst. The SOFIA spectra show no evidence for strong H or He I emission lines on day 87. However, the [O IV] 25.91 μm fine structure line, frequently seen in other novae (Gehrz et al. 2015; Evans & Gehrz 2012; Helton et al. 2012) is marginally detected. A Gaussian fit gives a line flux of 6.9 ± 1.6 W m^{-2}. The upper level of this line is collisionally de-excited at electron densities (n_e) in excess of 9.9×10^3 cm^{-3} (for an electron temperatures of 10^4 K); the presence of the line therefore indicates that the electron density in the region where the line is produced is less than this value.

4. Discussion

4.1. Reddening and Distance

In order to derive the reddening toward the system, we use the EWs of several absorption lines from diffuse interstellar bands, in combination with the empirical relations from Friedman et al. (2011). We derive an average $E(B-V) \approx 1.0 \pm 0.1$ mag and $A_V = 3.1 \pm 0.3$ mag for $R_V = 3.1$, in good agreement with the results of Geballe et al. (2019). We avoid

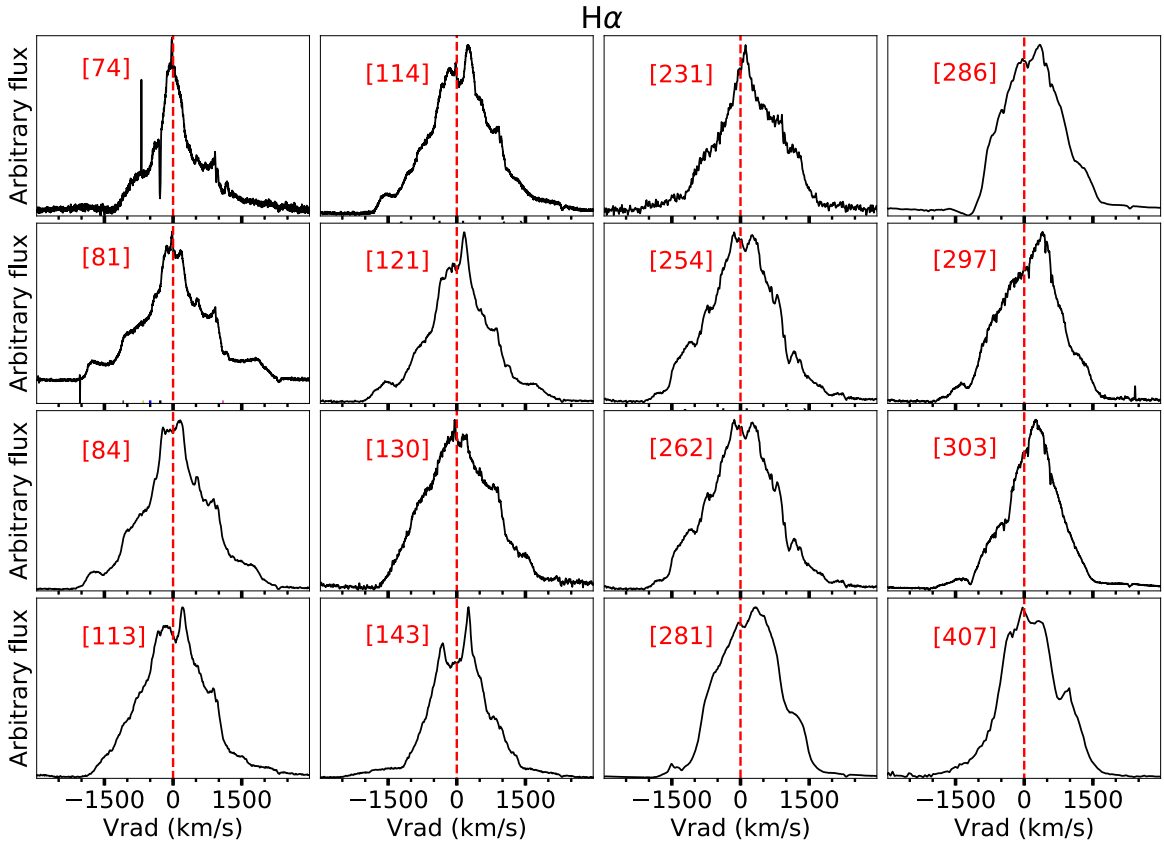

Figure 8. Line profile evolution of Hα throughout the outburst of V1047 Cen. The numbers between brackets are days after outburst. The red dashed lines represent the rest velocity ($V_{\rm vrad} = 0$ km s^{-1}). A heliocentric correction is applied to the radial velocities.

using the interstellar Na I D absorption doublet due to saturation. This is much smaller than the values derived from the Galactic reddening maps of Schlafly & Finkbeiner (2011), which estimate $A_V \approx 35$ mag toward the system. However, the measurements from Schlafly & Finkbeiner (2011)'s reddening maps should be considered an upper limit on the reddening along the line of sight. In addition, at Galactic latitude $< |5|^\circ$, which is the case for V1047 Cen, the reddening estimates of the maps are not reliable.

The Gaia parallax measurement of V1047 Cen suffers from large uncertainties. The latest Gaia EDR3 parallax of the system is 0.338 ± 0.249 mas (Gaia Collaboration et al. 2021). With a flat prior (Galactic latitude-based priors are not appropriate for novae), this implies a distance of $2.7^{+3.9}_{-1.0}$ kpc, which is not a useful constraint.

Due to the high uncertainty in the Gaia parallax, we use the three-dimensional Galactic reddening maps from Chen et al. (2019) and our measured reddening value to estimate the distance to V1047 Cen. The reddening map uses measurements from the Gaia DR2, Two Micron All Sky Survey (2MASS), and WISE surveys. Therefore, we converted the previously derived $E(B-V)$ measurement to reddening values in the 2MASS *JHK* filters and the Gaia DR2 G, G_{Bp}, and G_{Rp} bands, using the extinction law from Wang & Chen (2019) and Chen et al. (2019). We derive $E(G-K_s) = 2.2 \pm 0.1$, $E(G_{Bp}-G_{Rp}) = 1.3 \pm 0.1$, and $E(H-K_s) = 0.2 \pm 0.1$ mag. Using these reddening values, we derive an average distance of 3.2 ± 0.2 kpc, consistent with the Gaia parallax distance within its large uncertainties. The above uncertainty for the reddening-based distance likely underestimates the systematic uncertainties in this calculation.

4.2. Evolutionary Stage of the Secondary

The average V- and I-band magnitudes as measured by OGLE long after the nova, between 2013 and 2018, are $I = 17.1$ and $V = 17.5$ mag. The post-nova color index is then $(V-I) = 0.38 \pm 0.07$, implying $(V-I)_0 = -1.19$, which is bluer for a typical CV system, implying a potential contribution from ongoing nuclear burning on the WD. In Figure 15 we show the OGLE light curve during the 6 yr prior to the 2019 outburst. Adopting a distance of 3.2 kpc, $A_V = 3.1$ mag and $A_I = 1.46$ mag, we derive $M_V \approx 1.9$ mag and $M_I \approx 3.5$ mag during the post-nova period. In addition to the companion star, we also expect contributions from the accretion disk, hot spot, the 2005 nova nebula, and any possible ongoing nuclear burning. Therefore, using the optical magnitudes/colors between 2005 and 2019 to constrain the evolutionary stage of the companion star is not straightforward.

The system is not listed in the USNO-B1.0 catalog (Monet et al. 2003), and is not apparent in visual inspection of blue or red plates of the Digitized Sky Survey (DSS; Figure 15). Since the completeness level of USNO-B1.0 is roughly $V \sim 20.5$–21 mag, the absolute magnitude of the system during quiescence (pre-2005) should be $M_V > 5$ mag (at least 3 magnitudes fainter than the post-2005 nova brightness). This rules out anything more luminous than a main-sequence secondary and favors a typical CV system with an orbital period of the order of a few hours (Darnley et al. 2012). However, if the distance and

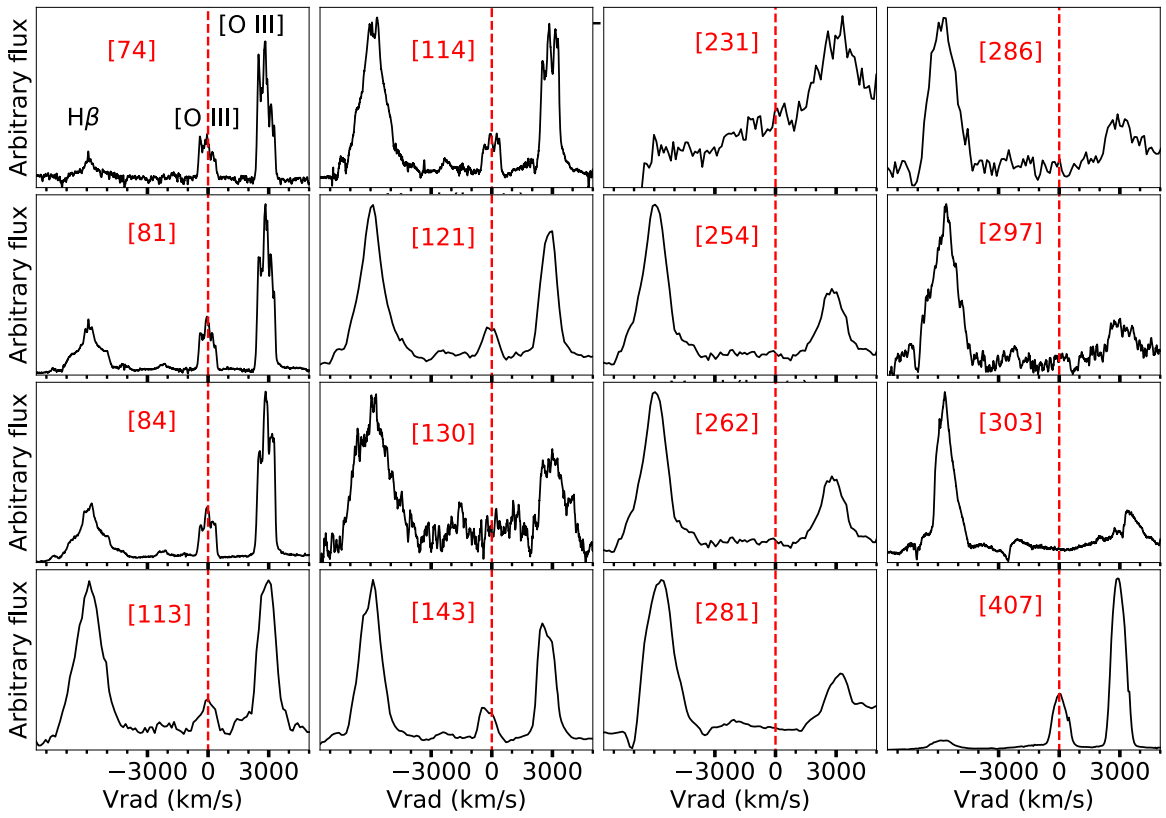

Figure 9. Evolution of the profiles of the O III lines at 4959 and 5007 Å in comparison to Hβ, throughout the outburst of V1047 Cen. The numbers between brackets are days after outburst. The red dashed lines represent the rest velocity ($V_{\rm vrad} = 0$ km s^{-1}) of O III 4959 Å. A heliocentric correction is applied to the radial velocities. Note that on day 231 Hβ falls near the end of the spectral range.

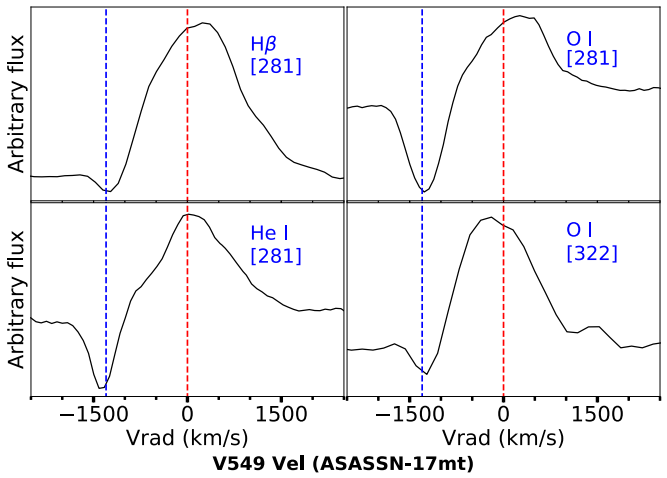

Figure 10. P Cygni line profiles of Hβ, He I 7065 Å, and O I 7773 Å taken on day 281 and O I 1.128 μm taken on day 323 (Numbers between brackets are days since t_0). The red and blue dashed lines represent $v_r = 0$ and -1300 km $^{-1}$, respectively.

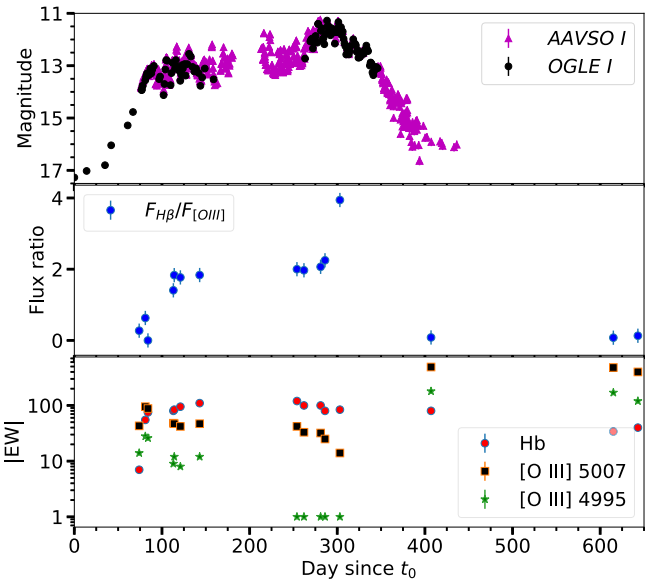

Figure 11. *Top*: the optical light curve in the *I* band. *Middle*: the evolution of the flux ratio between Hβ and O III 5007 Å. *Bottom*: the evolution of the EW of the Hβ, O III 5007 Å, and O III 4995 Å emission lines.

extinction we derive are underestimated, the secondary star might be more evolved; If we assume a distance $\approx$6 kpc (closer to the upper limit of the distance estimated from the Gaia parallax), and A_V 5 mag (note that the Schlafly & Finkbeiner 2011 maps estimate $A_V \approx 35$ mag in the direction of the system), we derive an absolute quiescent magnitude brighter than 2 magnitudes in the *V* band—implying a more evolved companion star (e.g., a subgiant).

4.3. The 2005 Eruption versus the 2019 Outburst

The 2005 nova eruption reached an apparent magnitude of around 8 mag in the visual, compared to a peak *V*-band magnitude of 13.5 for the 2019 outburst (Figures 1 and 2).

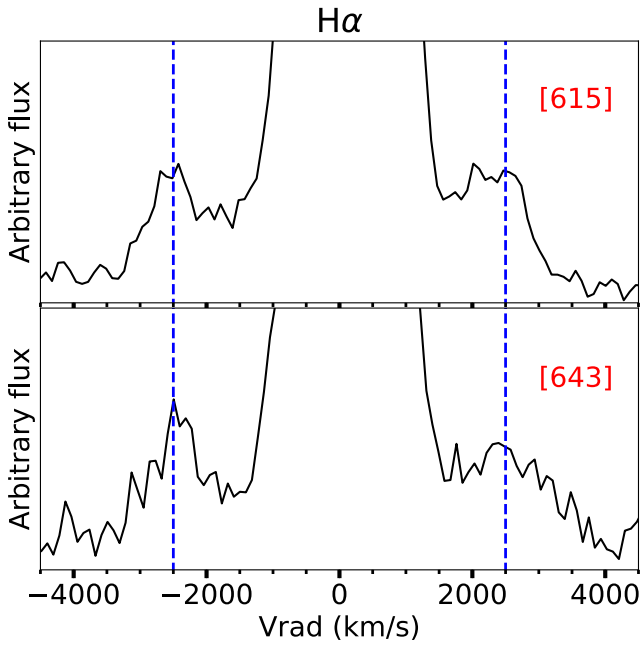

Figure 12. High-velocity *satellite* features in the late Hα line profiles, taken on days 615 and 643. The origin of these features is considered in the discussion in Section 4.

These translate to an absolute visual magnitude of ≈ -8 for the 2005 eruption and ≈ -2 for the 2019 outburst, using $A_V = 3.03$ and a distance of 3.2 kpc (see Section 4.1).

The energy radiated during the 2005 nova eruption can be estimated by integrating the Eddington luminosity of the WD over the period of the eruption. The Eddington luminosity of a 1 $M_\odot$ WD is of the order of 10^{38} erg s^{-1}. Novae emit close to Eddington (and in many cases super-Eddington) luminosity for months up to years (Starrfield et al. 2008). As a conservative estimate, we will assume emission at Eddington luminosity over 100 days. Note that the Swift follow-up of the 2005 nova event, 5 months after the discovery, showed hard X-ray emission which is typically detected prior to the X-ray supersoft phase (see, e.g., Gordon et al. 2021). Therefore, it is likely that the nova radiated at near Eddington luminosity for longer than 100 days. Over 100 days, the amount of energy radiated by the 2005 nova event is of the order of $\sim 10^{45}$ erg. This is only the energy radiated, but a considerable portion of the energy during a nova goes into kinetic energy of the ejecta (e.g., Gallagher & Starrfield 1976). Therefore, the energy output during the 2005 nova event is at least a few times 10^{45} erg—a very conservative estimate. For the 2019 outburst, determining the energy output is not straightforward, given that the event might be a combination of mechanisms, starting with a disk re-brightening, due to enhanced mass transfer or disk instability, leading to ejection of material.

There is no model that describes well the emission during the 2019 event; hence, given the lack of appropriate models, we will assume blackbody emission, which should be a fair assumption for the purpose of the rough estimates we are trying to derive. At a distance of 3.2 kpc and $A_V = 3.1$ mag, a blackbody with $T \approx 18{,}000$ K and $R \approx 1.5 \times 10^{11}$ cm should have an apparent V-band magnitude of ≈ 15.0. This is comparable to the average maximum V-band magnitude throughout the 2019 outburst. Such a blackbody has a bolometric luminosity of a few times 10^{36} erg s^{-1}. Assuming that this blackbody emission represents most of the luminosity, the total energy radiated during the 2019 outburst would be $\sim 10^{44}$ erg in 400 days. This could be an overestimate given that the peak average magnitude of ≈ 15.0 lasted for 200 days only and the outburst showed 100 days of rise and 100 days of decline. So, the actual energy radiated is possibly less than 10^{44} erg, based on the blackbody emission. But given the uncertainty on the bolometric correction and given that we do not take into account the kinetic energy of potential material ejection, we will assume 10^{44} erg to be a rough estimate for the total energy output of the 2019 outburst. This shows that the 2005 nova event is at least an order of magnitude more energetic than the 2019 outburst, proving that the two events are of distinct natures.

The morphology of the optical light curves is also distinctively different, with the 2005 light curve typical of a fast classical nova, while the light curve of the 2019 event plateaued at its peak for around a year. The velocities measured from the spectra taken during the 2005 eruption range from 750–1800 km s^{-1}. These velocities are slow to moderate in comparison to the velocities observed in classical novae. During the rise of the 2019 outburst, the velocities measured from some of the lines were around a few hundred kilometers per second (typical of CVs), but later in the outburst, the spectral lines showed velocities of ≈ 2000 km s^{-1}, raising more questions about the nature of this event.

4.4. The 2005–2019 Post-nova Period

In Figure 15, we show charts of the field of V1047 Cen from DSS (red plates taken in 1999 February), OGLE (taken in 2014 February), and SOAR (taken in 2019 June). Clearly, there is an excess in the brightness of the system in 2014, 9 yr after the 2005 nova eruption, compared to the pre-nova. This indicates that the system did not return to the pre-nova brightness.

The OGLE ($V - I$) colors between 2010 and 2019 indicate a blue source with high temperatures, in excess of 10^5 K. These substantially blue colors could be due to the contribution of emission lines to the spectra—particularly the [O III] lines from the nova nebula, whose fluxes contribute to the V band. These lines were relatively strong compared to the other lines during the early spectra of the 2019 outburst and after the end of the outburst (Figure 7). Unlike the V band, no strong nebular lines contribute to the flux in the I band (Figure A1).

Moreover, the blue colors (implying high temperatures) are likely an indication of ongoing nuclear burning on the surface of the WD. Many nova systems have shown extended supersoft X-ray emission and continued remnant thermonuclear burning on the surface of the WD several years after nova eruptions (e.g., Schaefer & Collazzi 2010; Zemko et al. 2015, 2016). This could be remnant burning from the accreted nova envelope or due to enhanced mass transfer from an irradiated secondary post-nova Ginzburg & Quataert (2021). Stable nuclear burning from enhanced accretion onto the WD has also been studied by Wolf et al. (2013). They derived the mass accretion rate needed for stable burning on a WD and found that, for WD masses between 0.6 and 1.3 $M_\odot$, the mass accretion rate should be of the order of $\sim 10^{-8}$–10^{-7} $M_\odot$ yr^{-1}.

We do not have definite estimates of the WD mass in V1047 Cen. Hachisu & Kato (2007) derived a low WD mass of around 0.7 $M_\odot$ for V1047 Cen, based on the light curve of the 2005 nova eruption. However, the values derived by Hachisu & Kato (2007) are uncertain, given that the light curve of

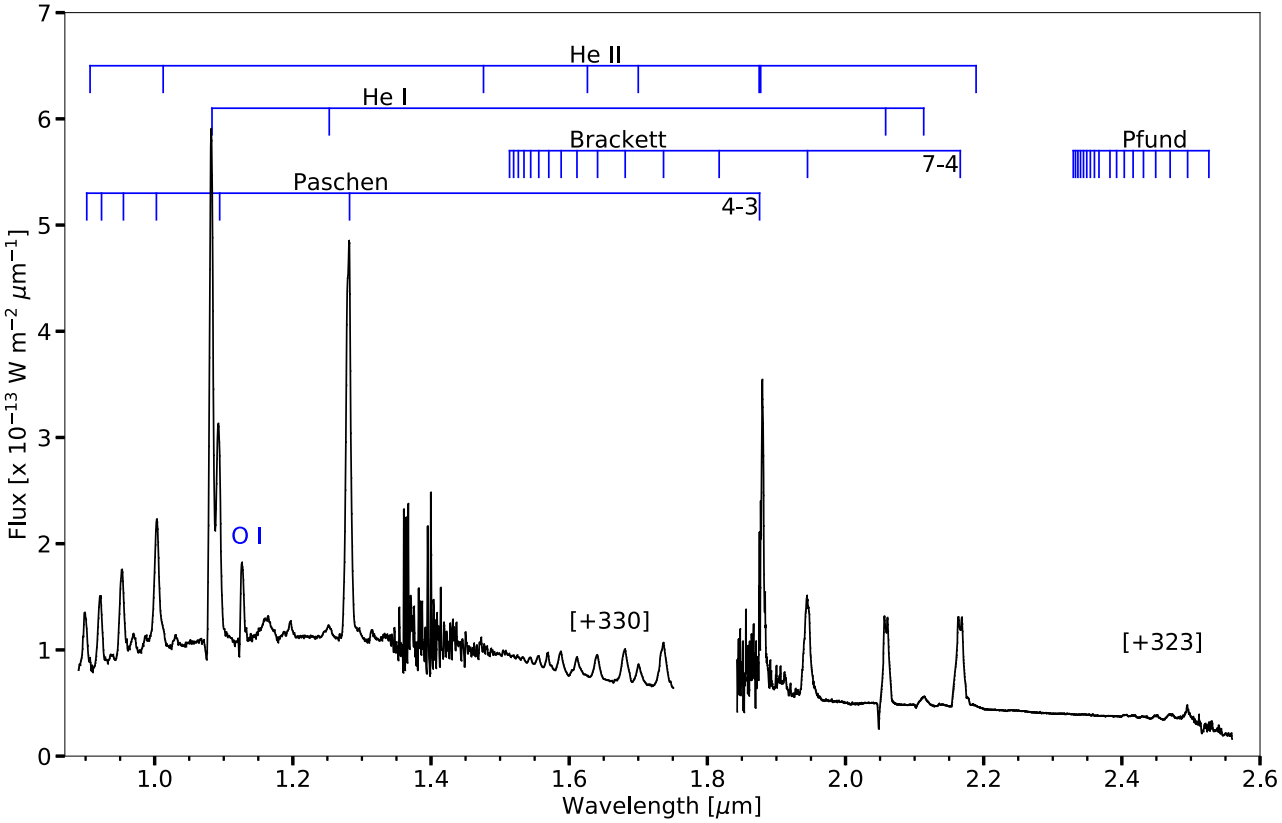

Figure 13. Gemini-S 0.9–2.5 μm spectra obtained on days 323 and 330. We identify hydrogen recombination and other He and O lines. For the recombination lines, we show the transition of the longest wavelength member.

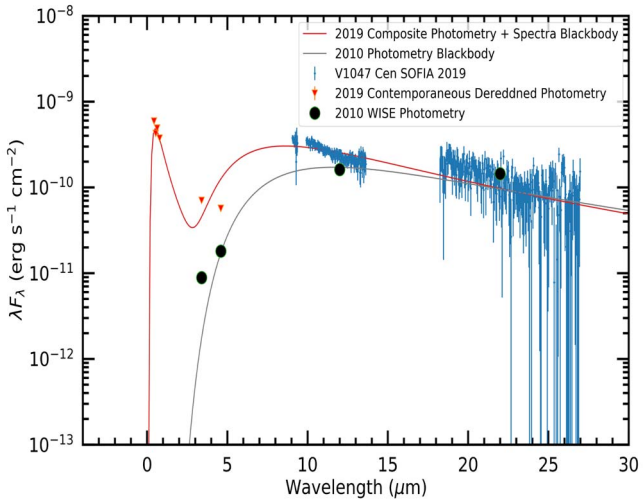

Figure 14. The 2019 SOFIA mid-infrared spectra of V1047 Cen obtained on day 87. The blue symbols represent the SOFIA spectra (combination of two grating settings G111 and G227), which include all spectral points where the atmospheric transmission at the flight altitudes are greater than 70% (hence, the gap near ~9.5 μm). The wavelength coverage of the two gratings is not continuous. Superposed is the best-fit composite blackbody (red solid line), i.e., the sum of a $T_{\rm bb} = 7070 \pm 950$ K from the 2019 photometry data plus a $T_{\rm bb} = 425 \pm 12$ K, the latter is interpreted as thermal emission from heated circumstellar material (dust) from the blast of the 2019 eruption. The inverted orange triangles are contemporaneous (2019) dereddened *BVRI* and NEOWISE photometry, while the filled-black circles are 2010 WISE photometry showing that the infrared SED peak was represented by a cooler blackbody (solid gray line) of $T_{\rm bb} = 315 \pm 30$ K.

V1047 Cen does not follow their *universal decline law*. On the other hand, the 2005 nova eruption of V1047 Cen showed a rapid decline in its optical light curve, which is indicative of an ejection of a low-mass envelope with large ejecta velocities (Starrfield et al. 2020); low-mass ejecta in turn tend to be associated with eruptions occurring on massive WDs (Yaron et al. 2005). Shara et al. (2018) combined simulations of nova eruptions with optical photometric data from Strope et al. (2010) and Schaefer (2010) to estimate the masses and accretion rates of WD stars in novae. Based on their relations and the parameters of the 2005 classical nova eruption of V1047 Cen—an eruption amplitude of ≈21–8.0 = 13 mag and a time to decline from the peak by 2 mag of $t_2 \approx 5$ days—we estimate a quiescent mass accretion rate of the order of 10^{-10}–$10^{-9}\,M_\odot$ yr^{-1} and a WD mass of around 1.2–1.4 $M_\odot$. This implies that V1047 Cen possibly has a massive WD. However, the ejecta velocities measured from the optical spectral lines during the 2005 classical nova are moderate (FWHM $<$ 2000 km s^{-1}; Liller et al. 2005), which argues against a massive WD (Shafter et al. 2011).

For a WD mass in the range of 1.2–1.4 $M_\odot$, the accretion rate needed for stable burning is a few times $10^{-7}\,M_\odot$ yr^{-1} (Wolf et al. 2013). This is relatively high for a typical accretion rate on a WD in a CV system. Even during a post-nova event, the mass-transfer rate is usually of the order of $10^{-8}\,M_\odot$ yr^{-1} (e.g., Kovetz & Prialnik 1985; Hillman et al. 2020). However, recent work by Ginzburg & Quataert (2021) showed that the post-nova mass accretion rate could be as high as $10^{-7}\,M_\odot$ yr^{-1} for several centuries. At such mass-transfer rate onto a massive

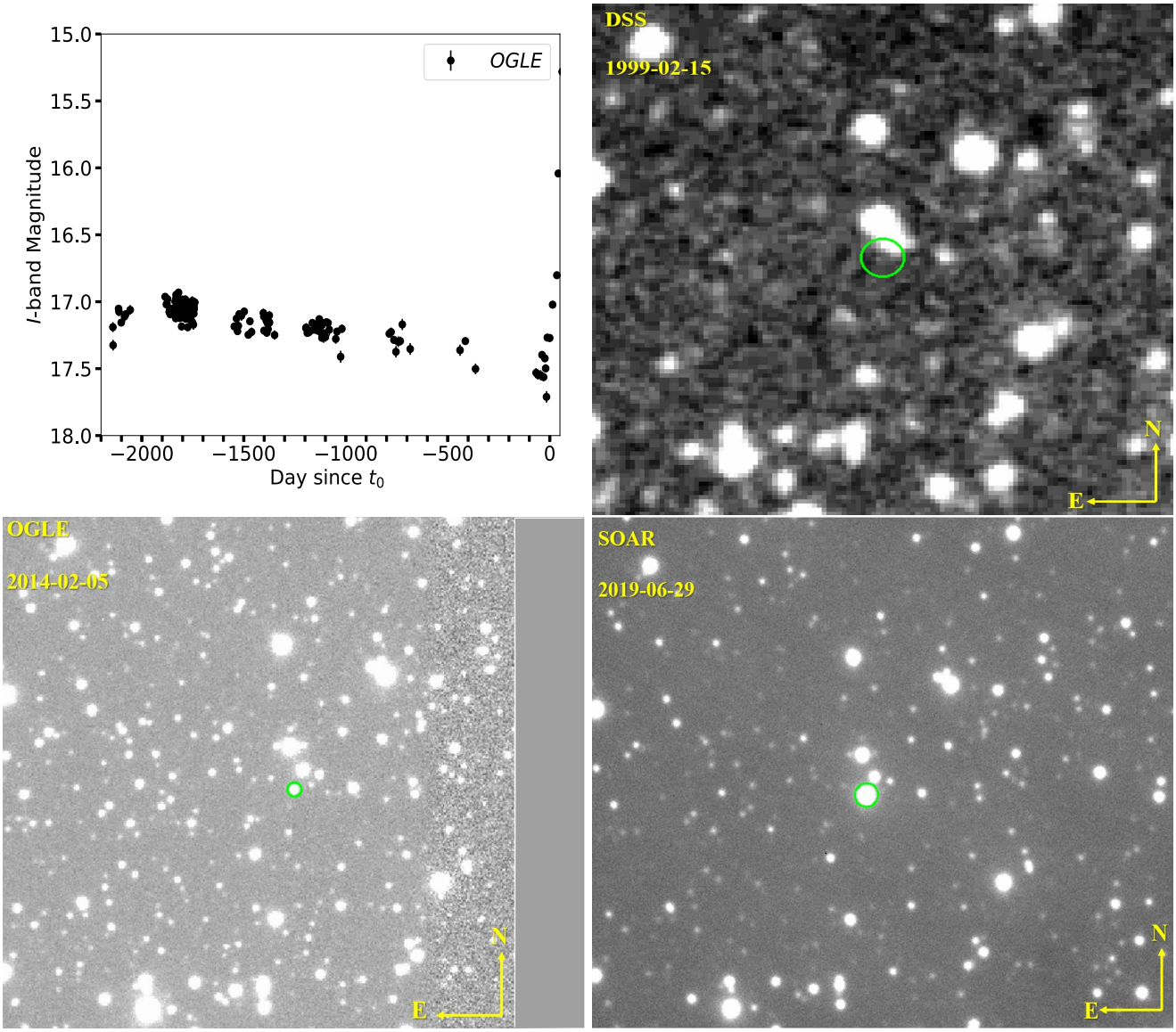

Figure 15. *Top-left:* the OGLE light curve between 2013 and 2019. Days are relative to the 2019 outburst start. *Top-right:* a red plate of the field of V1047 Cen from DSS obtained in February 1999 (position of V1047 Cen indicated by a green circle). *Bottom-left:* combined OGLE *I*-band images of V1047 Cen (circled in green) taken in February 2014. *Bottom-right:* SOAR unfiltered acquisition image of V1047 Cen (circled in green) taken in June 2019, during the 2019 outburst. In all the charts the field is $2' \times 2'$. V1047 Cen lies on the edge of the OGLE images, which is the reason why the chart is cropped on the west edge.

WD (1.2–1.4 $M_\odot$), the system would be a bright supersoft source (Wolf et al. 2013; Page et al. 2020), easily detectable with Swift at a distance of ∼3–4 kpc and with $A_V = 3.1$ (implying interstellar $N(H) = 8.7 \times 10^{21}$ cm^{-2}; Bahramian et al. 2015). However, there was no X-ray detection with Swift in 2008 nor throughout the 2019 outburst.

Another alternative is that the stable nuclear burning is taking place on a low-mass WD (0.6–0.8 $M_\odot$) with emission too soft to be detected with Swift. Stable burning on such a relatively low-mass WD would require a mass accretion rate of the order of 10^{-8} $M_\odot$ yr^{-1} (Wolf et al. 2013), which is a more typical post-nova mass-transfer rate. Similarly, the lack of X-ray detection during the 2019 outburst is an indication that—if nuclear burning is present during the 2019 outburst—it must be taking place on a low-mass WD rather than a high mass WD.

If the ongoing nuclear burning is from residual material from the nova eruption, this also means that the WD in nova V1047 Cen is of a low mass (0.6–0.8 $M_\odot$), for it to last for several years. The residual nuclear burning on a high mass WD after a nova eruption typically lasts for a few weeks/months only (e.g., MacDonald 1996; Schwarz et al. 2011).

Regardless of the mass of the WD, stable nuclear burning is likely taking place on the surface of the WD between 2005 and 2019, and is responsible for the post-2005-nova brightness excess compared to the pre-nova brightness and the substantially blue colors in the OGLE data between 2013 and 2019.

4.5. The 2019 Outburst of V1047 Cen—a Potential Record Breaker?

Only a few classical novae are known to have shown DN outbursts after a nova eruption, such as GK Per (Nova Persei 1901; Sabbadin & Bianchini 1983; Bianchini et al. 1986), V1017 Sgr (Nova Sagittarii 1919; Sekiguchi 1992; Salazar et al. 2017), and V446 Her (Nova Herculis 1960; Honeycutt et al. 1995, 2011; see Table A9 for a full list). The first DN

outbursts of these novae occurred several decades after the nova eruption, with the shortest gaps being 54 yr (V1017 Sgr), 47 yr (GK Per), and 30 yr (V446 Her). The 14 year gap between the classical nova eruption and the 2019 outburst of V1047 Cen is the shortest ever recorded, if it is indeed a DN outburst. Note that the older novae like GK Per and V1017 Sgr might have had earlier DN outbursts that were missed due to monitoring gaps.

During the 2019 outburst of V1047 Cen, the rise to the optical peak, plateau phase, and decline lasted 100, 210, and 100 days, respectively. This 400 day outburst is twice as long as the longest known DN outburst, previously recorded for V1017 Sgr and four times longer than the longest outburst recorded for GK Per (e.g., the 2006 outburst; Evans et al. 2009).

The peak absolute magnitude at the *V* band during the 2019 outburst reached ≈ -2 mag. This is higher than the typical absolute magnitudes of DNe during outburst, which range between 3.8 and 2.6 mag (Ramsay et al. 2017). Some systems with long periods (of the order of days), such as V1017 Sgr and V630 Cas, have extremely luminous DN outbursts, with absolute magnitudes reaching -0.3 and 1.4 mag, respectively. However, even these are still substantially less luminous compared to V1047 Cen. Therefore, if the 2019 outburst of V1047 Cen is a DN, it would be the most luminous outburst of a DN observed to date. Note that Kawash et al. (2021) showed that some DN outbursts could reach absolute magnitudes brighter than zero, but accurate distances and extinction values were unavailable for these systems in their study. As mentioned in Section 4.3 the peak luminosity of the 2019 outburst is more than a few times 10^{36} erg s, which is orders of magnitude larger than the typical luminosity of DNe ($\sim 10^{34}$ erg s; Warner 1995). At a few times 10^{36} erg s, the outburst is too energetic to be powered by accretion alone.

All the above indicate that the 2019 outburst of V1047 Cen is either a record breaking DN outburst or—more likely—a more energetic phenomenon than a disk instability event, as we discuss below.

4.6. Origin of the Spectral Features

During the rise phase (days 0–90), the spectrum of V1047 Cen resembled that of a DN superimposed on a spectrum of an old classical nova shell, implying an origin in a bright accretion disk. However, the subsequent evolution, particularly of the Balmer lines, differed considerably from that of DNe. The widths of the Balmer lines reached velocities much larger than those of the nova's nebular lines, with FWZIs of around 4000 km s^{-1} (compared to FWZIs $\approx$ 1100 km s^{-1} for the latter; see Figures 8 and 9). These velocities are also much larger than those measured for the Balmer lines during GK Per's recent outburst (FWHM $\sim$ 500–650 km s^{-1}; e.g., Wilber et al. 2015) or other DNe in outburst (Morales-Rueda & Marsh 2002). The Balmer lines also showed substantial increases in their line fluxes relative to the nova nebular lines more than 100 days into the 2019 outburst (Figure 9). The cause of this dramatic flux increase and broadening is not clear, but it is likely due to a fast, low-density outflow (given that these velocities are higher than the escape velocities of a 0.8–1.3 $M_{\odot}$ WD). All this indicates that, in addition to the early disk brightening, there are other mechanisms shaping the electromagnetic signatures of V1047 Cen.

Between days 262 and 310, most of the lines in the spectrum (e.g., Balmer, He I, and O I) showed P Cygni–like absorption features at velocities of around -1400 km s^{-1}. Such features are not characteristic of a DN outburst. They probably originate in an optically thick wind/outflow. The onset of these features coincides with the start of the brightness increase between days $\sim$260 and 310 (Figure 2), supporting the possibility of a wind or shell ejection during this phase of the outburst.

The satellite emission components at $\pm$2500 km s^{-1} in Hα around 7 months after the end of the outburst (Figure 12), are reminiscent of the features observed in Z And–like classical symbiotic outbursts. They are associated with collimated bipolar flows (see, e.g., Burmeister & Leedjärv 2007; Skopal et al. 2013; Tomov & Tomova 2013).

4.7. Origin of the Bright Radio Emission

In the past decade, CVs have been established as radio emitters during both quiescent and outburst phases (e.g., Córdova et al. 1983; Coppejans et al. 2015, 2016; Barrett et al. 2017). Their radio properties are diverse, and the emission mechanisms powering CV radio luminosity are still being established.

Coppejans et al. (2015) observed several nova-like CVs and found that they are significant radio emitters. Nova-like CVs are nonmagnetic CVs characterized by a sufficiently high mass-transfer rate to maintain the accretion disk in a constant hot state, unlike CV systems, which undergo DN outbursts. For the individual systems in their sample, Coppejans et al. (2015) found that the emission in these nova-like CVs is consistent with optically thick synchrotron, gyrosynchrotron, or cyclotron maser emission. Their 6 GHz spectral radio luminosities are $\sim 10^{15}$–10^{17} erg s^{-1} Hz^{-1} (Coppejans et al. 2015).

Nonmagnetic CVs, which undergo DN outbursts are also known to be radio sources during outburst (Coppejans et al. 2016). The most famous of these systems is SS Cyg, which shows a radio flare during the early days of its optical outbursts, peaking at $\sim$1 mJy before fading gradually, dropping below radio detectability by the end of the optical outburst. This flaring radio emission resembles that of X-ray binaries and is suggested to be the result of synchrotron emission from a transient jet (e.g., Körding et al. 2008; Miller-Jones et al. 2011; Russell et al. 2016; Coppejans et al. 2016; Coppejans & Knigge 2020). Coppejans et al. (2016) found that the radio spectral luminosities of DNe in outburst range between 10^{14} and 10^{16} erg s^{-1} Hz^{-1} at 10 GHz.

Based on a radio survey targeting a large sample of magnetic CVs, Barrett et al. (2017) suggest that they are also radio emitters, dominated by weakly polarized gyrosynchrotron emission or highly polarized electron-cyclotron maser emission. Most of these are nearby (less than a kiloparsec) sources and are characterized by flux densities, $\sim$20–400 μJy; the implication is radio spectral luminosities in the range $\sim 10^{14}$–10^{17} erg s^{-1} Hz^{-1} (Barrett et al. 2020). Only one of them, AE Aqr, shows substantially higher flux density ($\sim$5 mJy), but it is located remarkably nearby, at a distance of $\approx$90 pc (Ramsay et al. 2017).

Similar to the other observational features of V1047 Cen across the spectrum, the radio emission from this system is record breaking and puzzling. Assuming a distance of 3.2 kpc, the spectral luminosity of V1047 Cen at 2 GHz is $\sim 10^{19}$ erg s^{-1} Hz^{-1}. This means that V1047 Cen is at least

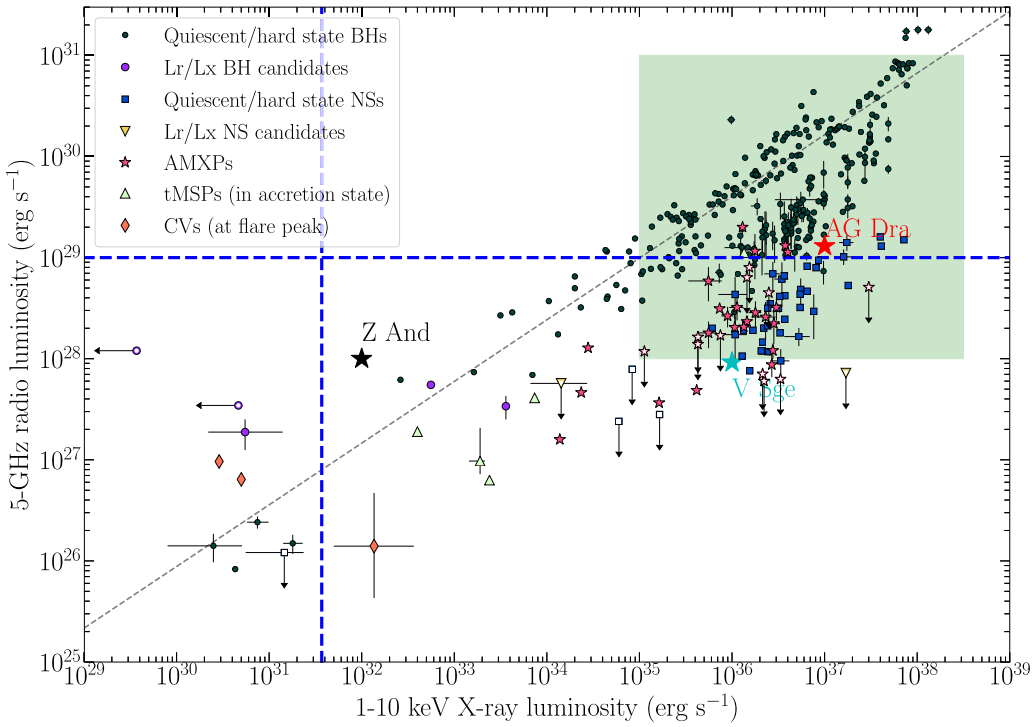

Figure 16. The plane of 5 GHz radio luminosity ($L_{\rm radio}$) vs. 1–10 keV X-ray luminosity ($L_{\rm X}$), with points representing X-ray binaries (accreting neutron stars, black holes), accreting and transitional millisecond pulsars, flaring CVs, classical novae, and classical symbiotics in outburst. The green shaded box represents the range of luminosities of classical novae. The classical symbiotics Z And and AG Dra are represented with black and red stars, respectively, while the X-ray binary V Sge is represented with a cyan star. The radio luminosity of V1047 Cen at 5 GHz is plotted with a dashed blue horizontal line and is calculated assuming a flat spectrum. Adopted from Bahramian et al. (2018) https://zenodo.org/record/1252036/export/hx.

two orders of magnitude brighter at radio wavelengths than all other CVs.

If the radio emission from a DN outburst is an optically thick thermal emission from ionized gas at a typical brightness temperature of 10^4–10^5 K, then the emitting regions should have radii of $\sim10^{14}$–10^{15} cm (assuming circular sources as projected on the sky) to produce the observed flux densities in V1047 Cen. During a DN outburst, it is reasonable to assume that the emitting gas has a size roughly equivalent to the size of the binary. CVs with orbital periods of the order of a few hours have orbital radii of $\sim10^{11}$ cm, which is three orders of magnitude smaller in size than the optically thick emitting gas responsible for the observed fluxes. This implies that if the outburst is a DN, any emission of order the size of the orbit must be nonthermal (brightness temperature $>10^5$ K).

One possibility is that the radio emission is nonthermal synchrotron emission from a transient radio jet, similar to the case of other DN outbursts. While the flux density of V1047 Cen equals that of SS Cyg during its short-lasting flare, the luminosity of V1047 Cen is several orders of magnitude brighter than that of SS Cyg (the distance to SS Cyg is 114 pc; Miller-Jones et al. 2013). In Figure 16 we plot V1047 Cen on the $L_{\rm radio}$ versus $L_{\rm X}$ diagram in comparison with jet emission in other CVs, classical novae, Z And, V Sge, and other astrophysical objects, such as X-ray binaries, accreting millisecond X-ray pulsars, and transitional millisecond pulsars (we multiply the spectral luminosity by 5 GHz to estimate the radio luminosity at 5 GHz assuming a flat spectrum). V1047 Cen's 5 GHz luminosity, $\sim1\times10^{29}$ erg s^{-1}, is much higher than that observed in CVs and is comparable to (or even brighter in some cases than) X-ray binaries and pulsars with compact primaries, like neutron stars and black holes. Such an energetic jet should also be a bright X-ray source. We used WebPIMMS[33] to derive the X-ray unabsorbed flux using the stacked Swift X-ray detection of the 2019 outburst and assuming a 5 keV thermal bremsstrahlung model and $N(H) = 8.7\times10^{21}$ cm^{-2} (we use $N(H) = 2.81\times10^{21}\,A_V$; Bahramian et al. 2015). This translates to an X-ray luminosity of around 3.7×10^{31} erg s^{-1} at a distance of 3.2 kpc, which is comparable to the X-ray luminosity of other CVs in outburst.

It is not possible to determine if V1047 Cen showed flaring radio emission during the early days of the outburst like SS Cyg and was an even brighter radio source at that time, or if the $\sim$1 mJy emission remained more or less constant throughout the optical outburst. Nevertheless, what is really puzzling is that at the end of the optical outburst, the radio flux did not drop. This is in contrast to the trends shown by SS Cyg and other DN outbursts, where the radio flux drops below the detection limit by the end of the optical outburst (Russell et al. 2016). This disparity between the radio behavior and energetics of V1047 Cen and other DN outbursts raises additional questions about the origin of the radio emission in V1047 Cen and if a transient synchrotron jet is an appropriate explanation.

Bode et al. (1987) conducted a radio survey of 26 classical novae observed with the VLA less than 10 yr after the eruption and detected only two in the sample. Both novae were detected at 5 GHz, 2 yr (V4077 Sgr) and 8 yr (NQ Vul) after the nova eruptions. The emission from these two novae was suggested to be thermal and had radio spectral luminosities $\sim10^{18}$–10^{19} erg s^{-1} Hz^{-1}. The higher-end radio spectral luminosity of V4077 Sgr is due to the fact that the system was observed only

[33] https://heasarc.gsfc.nasa.gov/cgi-bin/Tools/w3pimms/w3pimms.pl

2 yr after the nova eruption; radio emission from classical novae often peaks on timescales ∼1–3 yr after the eruption (Chomiuk et al. 2021b). In addition, given that radio emission from decade-old or older nova ejecta originates in the nova's extended thermal remnant, it can vary only slowly, not on the weeks–months timescales observed in V1047 Cen (Chomiuk et al. 2021b). Therefore, it is very unlikely that the radio emission from V1047 Cen originates in the ejecta of the 2005 classical nova eruption.

The long-lasting, luminous radio emission in V1047 Cen resembles the radio emission from Z And–like classical symbiotic, accretion-powered, outbursts (e.g., Crocker et al. 2001; Mikołajewska 2002; Brocksopp et al. 2004; Sokoloski et al. 2006). These systems are luminous radio sources ($L \approx 10^{18}$–10^{19} erg s^{-1} Hz^{-1}; Ogley et al. 2002; Brocksopp et al. 2004), where the emission is usually suggested to be thermal, originating from bipolar collimated jets/outflows. Classical symbiotic systems consist of giant stars, which in most cases do not fill their Roche Lobes, transferring material onto WDs; accretion can proceed via a disk or not, depending on the relative velocity of the red giant wind and the accreting WD (Livio 1992; Mohamed & Podsiadlowski 2007). Even out of outburst, symbiotic stars can be luminous radio emitters ($L \approx 10^{17}$–10^{20} erg s^{-1} Hz^{-1}), as the hot accreting WD ionizes the substantial circumstellar material expelled by the giant companion (Seaquist et al. 1984; Seaquist & Taylor 1990; Mikołajewska 2012).

We showed earlier that if the radio emission is optically thick thermal emission from ionized gas at a typical brightness temperature of 10^4–10^5 K, the emitting regions should have a radius of $\sim 10^{14}$–10^{15} cm to produce the observed flux densities. If the radio emission observed from V1047 Cen proves to be transient and associated with the 2019 outburst, it might be attributed to outflows moving at velocities $\gtrsim$2000 km s^{-1} (based on the optical line profiles), which will cover a radius of more than 10^{15} cm in less than 2 months. The variability of the radio source can then be explained as variability in the fast outflow.

4.8. The Nature of the Outburst

The spectroscopic follow-up of V1047 Cen during the rise to peak (first 90 days) and the low amplitude of the outburst are fairly consistent with a DN outburst; however, the 400 day long outburst, the 14 yr gap between the 2005 nova eruption and the 2019 outburst, the luminous radio and optical emission, the dramatic spectral changes and high-velocity spectral components are not consistent with a DN and raise questions about the nature of this event. In addition, the amplitude of the outburst (≈6 mag), the absolute peak magnitude, and the spectral evolution are not consistent with a classical nova event. Moreover, there is a striking difference between the 2005 classical nova and the 2019 outburst. All this suggests that the 2019 outburst of V1047 Cen is unique and is not consistent with common phenomena observed in CV systems, such as DNe and classical novae. A definitive explanation for what happened during the 2019 outburst has not yet arisen based on the current data set, but we offer below several potential scenarios, while listing their pros and cons.

Many of the features observed in V1047 Cen resemble those of Z And–like classical symbiotic outbursts (Sokoloski et al. 2006). This type of event starts with a disk instability outburst, leading to the accretion of a massive accretion disk onto the WD. The accretion burst is large enough to trigger enhanced nuclear burning on the surface of the WD and the ejection of an optically thick outflow/shell (see also Munari 2019).

While classical symbiotic systems are characterized by orbital periods of the order of hundreds of days (Mikołajewska 2003; much longer than the potential few hours orbital period in V1047 Cen), the observational features of classical symbiotic outbursts have similarities with those of V1047 Cen (the long-lasting optical outburst, the long-lasting, and luminous radio emission, the P Cygni spectral features with velocities of ≈1500–2000 km s^{-1}, the high ionization lines in the optical spectra, and the late satellite spectral features around the Balmer lines indicative of bipolar flows).

Therefore, one of the possibilities is that the 2019 outburst of V1047 Cen is similar in nature to classical symbiotic outbursts, starting with a DN disk instability type outburst (based on the early optical spectra), leading to the accretion of the entire accretion disk onto the WD. The accretion of the disk might have led to enhanced nuclear shell burning on the surface of the WD, which launched a radiation-driven wind/outflow (Sokoloski et al. 2006). This scenario could explain the 400 day outburst duration in the optical (e.g., the 2000 outburst of Z And lasted for 2 yr) and the dramatic brightening and broadening of the Balmer lines. The light-curve bump or re-brightening that occurred ∼250 days after the outburst start could mark the stage at which an optically thick outflow started. This is consistent with the development of P Cygni–like absorption features in the optical spectral lines around the same period (Figure 10). The absence of the P Cygni profiles in the spectra obtained on day 407 after the end of the optical outburst (Figure 7; note that the P Cygni profiles were present in the previous epoch on day 303) indicates that the optically thick wind/outflow dissipated rapidly and became optically thin, which is very similar to the behavior observed in the outburst of Z And (Sokoloski et al. 2006). The presence of high ionization lines of He, C, O, N, and potentially forbidden Fe in the late spectra of V1047 Cen (Figure A6), obtained after the end of the optical outburst could indicate ongoing nuclear shell burning, which would strengthen the case for this scenario, which transitions from an accretion-powered outburst to a nuclear-powered outburst. The same high ionization lines of N V and O VI are typically observed in V Sge–like stars (the Milky Way counterparts of the supersoft sources in the Magellanic Clouds), and typically indicate nuclear shell burning (e.g., Herbig et al. 1965; Cieslinski et al. 1999; Steiner et al. 1999; Starrfield et al. 2004). Sokoloski et al. (2006) derived the luminosity of Z And a good part of the 2006 outburst to be of the order of 10^{36} erg s, which is close to the luminosity of V1047 Cen during the flat peak phase of the 2019 outburst.

This scenario could also explain the long-lasting, luminous radio emission. We showed in Section 4.7 that the flux densities observed in V1047 Cen could be explained as thermal emission from an outflow of ionized gas. Such radio emitting outflows/jets are characteristics of classical symbiotic outbursts (e.g., Brocksopp et al. 2004 and references therein). In addition, there is strong evidence for the presence of such collimated outflows or jets in V1047 Cen based on the satellite emission components observed in Hα (Figure 12), which are similar to those observed in Z And–like classical symbiotic outbursts (e.g., Munari et al. 2005; Burmeister & Leedjärv 2007; Skopal et al. 2013;

Tomov & Tomova 2013). The bright radio emission in Z And–like systems, is mostly due to the presence of dense circumstellar material from the evolved secondary, ionized by the outburst on the WD. However, for a system like V1047 Cen, which likely hosts a dwarf companion, we do not expect a dense circumstellar environment. Unless, the medium around the system has been enriched by material from a swelled companion after the 2005 nova, during a phase of enhanced mass transfer, coupled with mass loss from the system. While there is no explanation for why this happens in a system like V1047 Cen specifically, it is within our attempts to explain the uniqueness of this outburst.

If strong internal shocks are not present within the outflow, bright X-ray emission might not be present, because the X-ray emission associated with the nuclear burning on a low-mass WD (see Section 4.4) would be hidden by the interstellar column density along with the puffed up photosphere and outflow during the outburst. This could explain the lack of X-ray detection in the Swift individual observations.

The energy radiated during the 2019 outburst is likely powered by different mechanisms (e.g., disk brightening and nuclear burning), making it difficult to estimate (see Section 4.3). However, if we assume that all ($\sim 10^{44}$ erg) the energy radiated is powered by nuclear burning, the mass needed to be accreted between 2005 and 2019 to power the 10^{44} erg would be around $1.6 \times 10^{-8}\,M_{\odot}$ of hydrogen, assuming a 0.7% nuclear burning efficiency (Clayton 1968). This amount of material could be accreted onto the WD with a moderate post-nova mass-transfer rate ($\sim 10^{-9}$–$10^{-8}\,M_{\odot}$ yr^{-1}.)

While a scenario similar to a classical symbiotic outburst could indeed explain some of the observational features during the 2019 outburst, this scenario suffers from some weaknesses. Sokoloski et al. (2006) suggest that preexisting quasi-steady shell burning on the WD surface is necessary to trigger a classical symbiotic nova. As mentioned earlier, the OGLE photometry between 2013 and 2019 indicates that quasi-stable nuclear burning on the WD surface could indeed have been ongoing prior to the 2019 outburst, with a mass accretion rate of the order of $10^{-8}\,M_{\odot}$ yr^{-1}, or remnant mass from the 2005 nova event. However, this mass accretion rate is high for a disk instability event to take place at the beginning of the 2019 outburst of V1047 Cen. While some systems, like GK Per and V1017 Sgr showed DN outbursts, just a few decades after a nova eruption when the accretion rate is expected to be of the order of $10^{-8}\,M_{\odot}$ yr^{-1}, these systems are characterized by long orbital periods (>1 day) and therefore potentially massive accretion disks, where a disk instability event could take place despite the high accretion rate. Similarly, Z And–like systems are characterized by high mass accretion rates ($\sim 10^{-8}\,M_{\odot}$ yr^{-1}) in long orbital period systems, harboring massive disks. However, if V1047 Cen is characterized by an orbital period of less than 10 hr, a disk instability would be more difficult to take place at this high mass accretion rate.

Moreover, the potential ongoing nuclear burning on the WD surface will heat up the disk to temperatures where a disk instability is not possible to occur. If the system brightness ($M_V \approx 1.9$ mag) prior to the 2019 outburst is mostly contributed by the nuclear burning irradiating the disk, this means that the disk temperature could reach over 10,000 K, implying that disk instabilities are not possible. Therefore, despite the early spectra's consistency with a DN outburst (Balmer and He I lines with FWHM of a few 100 km s^{-1} and strong He II at 4868 Å), a disk instability may not be the trigger of the 2019 outburst. In addition, the optical light curve of V1047 Cen is of higher amplitude compared to typical light curves of classical symbiotic outbursts. For example, the 2006 outburst of Z And reached an amplitude of 2–3 mag compared to more than 6 magnitudes in V1047 Cen. However, it is worth noting that the amplitude of the outburst is not only related to the outburst radiated energy, but also the magnitude of the companion star. Since the companion star in Z And is a bright, giant star, the amplitudes of the outbursts in such systems are expected to be low.

If the distance and reddening estimate toward V1047 Cen are larger than the ones we derive, this would imply that the companion star is an evolved one (e.g., a subgiant; see Section 4.2). If so, this would place V1047 Cen in the same category as GK Per and V1017 Sgr, i.e., systems characterized by a large disk and an orbital period larger than 1–2 days. This implies that a disk instability could still take place despite a large mass-transfer rate. Moreover, even if the inner parts of the disk are characterized by temperatures in excess of 10^4 k, the outer parts of the large disk could be cold enough for instability to happen.

Based on the early spectral features, a disk brightening likely took place during the early weeks of the outburst. If this did not happen due to an instability in the disk, an alternative possibility is that the disk brightened due to enhanced mass-transfer rate from the companion. Bollimpalli et al. (2018) suggested that for the 2000–2002 outburst of Z And, a disk instability could not be the trigger of the outburst. This is mainly due to the irradiation of the disk by the hot WD, implying that a DN would only be significant at very high mass-transfer rates ($10^{-6}\,M_{\odot}$ yr^{-1}), which is higher than the typical mass-transfer rate in such systems. Bollimpalli et al. (2018) suggest that the outburst of Z And between 2000 and 2002 might have been triggered by a mass-transfer enhancement from the giant companion, leading to an increase in nuclear burning on the WD surface. It could be that something similar took place during the early stages of the 2019 outburst of V1047 Cen. However, based on the colors of V1047 Cen prior to 2019, there is evidence for ongoing nuclear burning on the WD surface, likely caused by post-nova enhanced mass-transfer rate. Therefore, we do not have a definitive explanation for what could lead to further enhancing the mass-transfer rate from the secondary into the surface of the WD.

One other possible explanation for the 2019 outburst is that the system experienced a non-ejection nova event. The extended grid of nova models by Yaron et al. (2005) shows that some combinations of parameters might lead to a thermonuclear runaway without ejecting material (see also Fujimoto 1982; Shara et al. 1977). Yaron et al. (2005) suggest that such outbursts cause only a slow increase in luminosity, followed by a slow decay, particularly in the case of low-mass WDs where the timescales of the rise and decay could be thousands of days. The supersoft X-ray transient ASASSN-16oh has been suggested to be a thermonuclear runaway event without mass ejection (Hillman et al. 2019). The system showed a slowly rising (1585 days) and declining (268 days) optical light curve, with an amplitude of less than 4 magnitude. While there are similarities between the optical light curves of ASASSN-16oh and V1047 Cen, the former has been detected as a supersoft X-ray source at the distance of the Small Magellanic Cloud. This is very different from the case of V1047 Cen, which was not detected in individual epochs by

Swift during the 2019 outburst despite our extensive monitoring. In the case of a thermonuclear runaway, the luminosity of the supersoft source is expected to be of the order of 10^{38} erg s^{-1}, which would have been easily observed at a distance of 3.2 kpc by Swift, if the WD is of higher mass ($>1\,M_{\odot}$). The supersoft emission of ASASSN-16oh was characterized by a luminosity of around 10^{37} erg s^{-1}, which is lower than that expected from the models of non-ejecting thermonuclear runaways. This low luminosity has been attributed to an optically thick accretion disk hiding most of the WD surface. While a massive accretion disk could also be blocking some of the emission from the WD surface in the case of V1047 Cen, it is a less likely possibility given the Swift nonindividual detections over several months. Moreover, the optical spectral evolution is consistent with the presence of an optically thick ejection/outflow. Therefore, a non-ejection nova scenario is less likely.

In conclusion, the 2019 outburst of V1047 Cen does not resemble the common events that take place in CV systems (e.g., DNe and classical novae). Based on the multiwavelength observational features, the outburst is likely the combination of multiple mechanisms, starting with a disk brightening, followed by the generation of an outflow. Such a unique outburst has never before been observed in a CV system that has experienced a recent classical nova eruption, indicating the possibility that we have witnessed a new astronomical phenomenon.

5. Conclusions

We have presented multiwavelength observations of the 2019 outburst in the 2005 classical nova V1047 Cen. The outburst amplitude reached around 6 magnitudes in the optical and lasted for more than 400 days. We derive a distance of 3.2 ± 0.2 kpc to the system and a peak absolute magnitude of the outburst $M_V = -2$, placing it between novae and DNe. The first spectra we obtained of the system around 74 days after the start of the outburst were consistent with a disk instability DN event in a classical nova system. If V1047 Cen is a DN, the event would be a record breaker, making it the longest DN outburst on record, the shortest gap between a nova and DN in a CV system, and the most luminous optical and radio DN outburst. This, along with the different observational features across the electromagnetic spectrum point toward a phenomenon more exotic than just a DN outburst.

We therefore suggest that the event is a combination of multiple mechanisms, starting with a brightening in the disk (due to enhanced mass transfer or less likely an instability in the disk), which then triggered enhanced nuclear shell burning on the surface of the WD and eventually led to an optically thick, radiation-driven wind/outflow. This scenario fits well the 400 day outburst duration, the dramatic changes in the optical line profiles and the >2000 km s^{-1} velocities inferred from these profiles, the P Cygni line profiles that appeared several months after the outburst start, the high peak optical brightness, and most importantly the long-lasting, superluminous radio emission that likely originates from ionized gas (thermal emission) in collimated bipolar flows, which are characteristic of classical symbiotic outbursts. Strong evidence for such outflows can be seen in the late optical spectral line profiles. Mid-infrared observations also indicate that preexisting dust—likely formed during the 2005 classical nova eruption—has been heated by the radiation from the 2019 outburst.

Therefore, the 2019 outburst of V1047 Cen is a unique phenomenon observed for the first time in a typical CV system, characterized by a short (∼hours) orbital period and which has undergone a recent classical nova eruption.

Support for this work was provided by NASA through the NASA Hubble Fellowship grant HST-HF2- 51501.001-A awarded by the Space Telescope Science Institute, which is operated by the Association of Universities for Research in Astronomy, Inc., for NASA, under contract NAS5-26555. We thank B. Schaefer for useful discussion. We thank the AAVSO observers from around the world who contributed their magnitude measurements to the AAVSO International Database used in this work.

E.A., L.C., and K.V.S. acknowledge NSF award AST-1751874, NASA award 11-Fermi 80NSSC18K1746, and a Cottrell fellowship of the Research Corporation. J.S. was supported by the Packard Foundation. D.A.H.B. gratefully acknowledges the receipt of research grants from the National Research Foundation (NRF) of South Africa. P.A.W. kindly acknowledges the National Research Foundation and the University of Cape Town. K.L.P. acknowledges funding from the UK Space Agency. Nova research at Stony Brook University has been made possible by NSF award AST-1611443. M.G. is supported by the EU Horizon 2020 research and innovation program under grant agreement No. 101004719. A part of this work is based on observations made with the Southern African Large Telescope (SALT), with the Large Science Programme on transients 2018-2-LSP-001 (PI: DAHB). Polish participation in SALT is funded by grant No. MNiSW DIR/WK/2016/07. This paper was partially based on observations obtained at the Southern Astrophysical Research (SOAR) telescope, which is a joint project of the Ministério da Ciência, Tecnologia e Inovações (MCTI/LNA) do Brasil, the US National Science Foundation's NOIRLab, the University of North Carolina at Chapel Hill (UNC), and Michigan State University (MSU). The OGLE project has received funding from the National Science Centre, Poland, grant MAESTRO 2014/14/A/ST9/00121 to AU. The CHIRON and *Andicam* instruments are managed by the Todd Henry and the SMARTS Consortium. The MeerKAT telescope is operated by the South African Radio Astronomy Observatory, which is a facility of the National Research Foundation, an agency of the Department of Science and Innovation. We acknowledge the use of the ilifu cloud computing facility—www.ilifu.ac.za, a partnership between the University of Cape Town, the University of the Western Cape, the University of Stellenbosch, Sol Plaatje University, the Cape Peninsula University of Technology and the South African Radio Astronomy Observatory. The ilifu facility is supported by contributions from the Inter-University Institute for Data Intensive Astronomy (IDIA—a partnership between the University of Cape Town, the University of Pretoria and the University of the Western Cape), the Computational Biology division at UCT and the Data Intensive Research Initiative of South Africa (DIRISA). This research is based in part on observations obtained at the international Gemini Observatory, a program of NSF's NOIRLab, which is managed by the Association of Universities for Research in Astronomy (AURA) under a cooperative agreement with the National Science Foundation. on behalf of the Gemini Observatory partnership: the National Science Foundation (United States), National Research Council (Canada), Agencia

Nacional de Investigación y Desarrollo (Chile), Ministerio de Ciencia, Tecnología e Innovación (Argentina), Ministério da Ciência, Tecnologia, Inovações e Comunicações (Brazil), and Korea Astronomy and Space Science Institute (Republic of Korea). D.P.K.B. is supported by a CSIR Emeritus Scientist grant-in-aid, which is being hosted by the Physical Research Laboratory, Ahmedabad. This work is based in part on observations made with the NASA/DLR Stratospheric Observatory for Infrared Astronomy (SOFIA). SOFIA is jointly operated by the Universities Space Research Association, Inc. (USRA), under NASA contract NNA17BF53C, and the Deutsches SOFIA Institut (DSI) under DLR contract 50 OK 0901 to the University of Stuttgart. Financial support for CEW/RDG related to this work was provided by NASA through award SOF07-0005 issued by USRA to the University of Minnesota. This publication makes use of data products from the Near-Earth Object Wide-field Infrared Survey Explorer (NEOWISE), which is a joint project of the Jet Propulsion Laboratory/California Institute of Technology and the University of Arizona. NEOWISE is funded by the National Aeronautics and Space Administration. VARMR acknowledges financial support from the Fundação para a Ciência e a Tecnologia (FCT) in the form of an exploratory project of reference IF/00498/2015/CP1302/CT0001, and from the Ministério da Ciência, Tecnologia e Ensino Superior (MCTES) through national funds and when applicable co-funded EU funds under the project UIDB/EEA/50008/2020, and supported by Enabling Green E-science for the Square Kilometre Array Research Infrastructure (ENGAGE-SKA), POCI-01-0145- FEDER-022217, and PHOBOS, POCI-01-0145-FEDER029932, funded by Programa Operacional Competitividade e Internacionalização (COMPETE 2020) and FCT, Portugal. The analysis made significant use of PYTHON 3.7.4, and the associated packages NUMPY, MATPLOTLIB, SEABORN, SCIPY. Data reduction made significant use of

Software: MIDAS FEROS (Stahl et al. 1999), echelle (Ballester 1992), PySALT (Crawford et al. 2010), IRAF (Tody 1986, 1993), ELEANOR (Feinstein et al. 2019), OGLE pipeline (Udalski et al. 2015).

Appendix
Supplementary Plots and Tables

In this Appendix we present supplementary plots and tables.

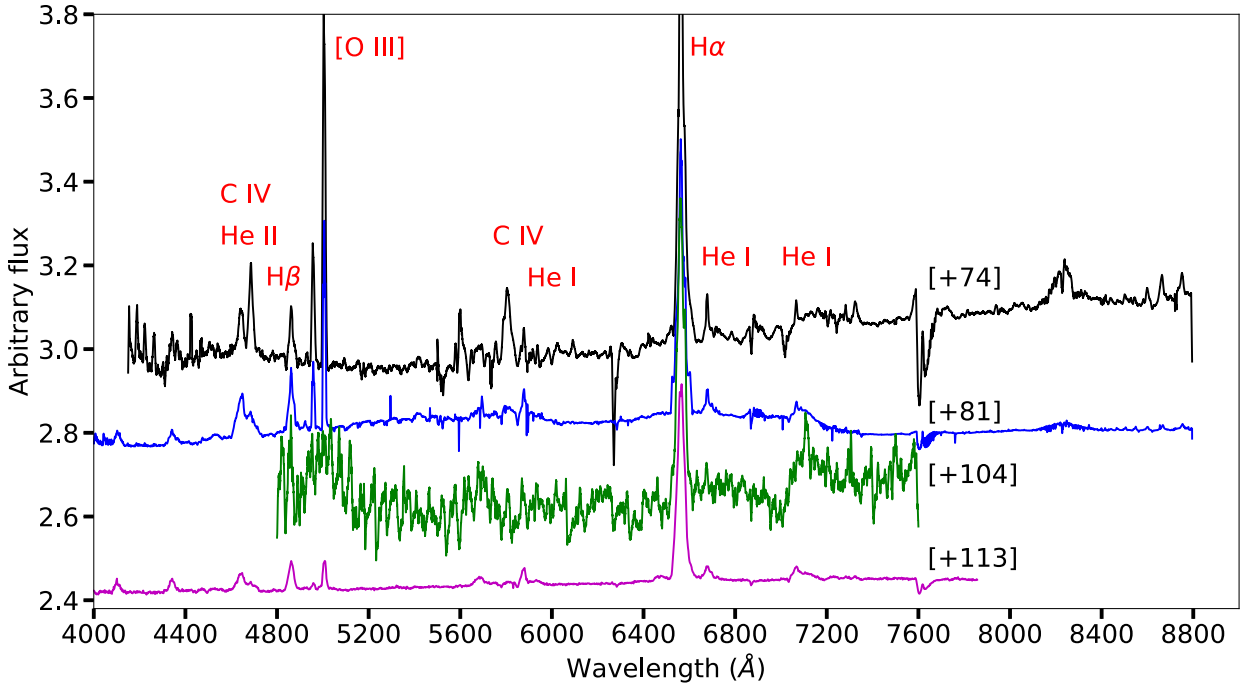

Figure A1. Optical spectral evolution of V1047 Cen. The numbers in brackets are days since t_0.

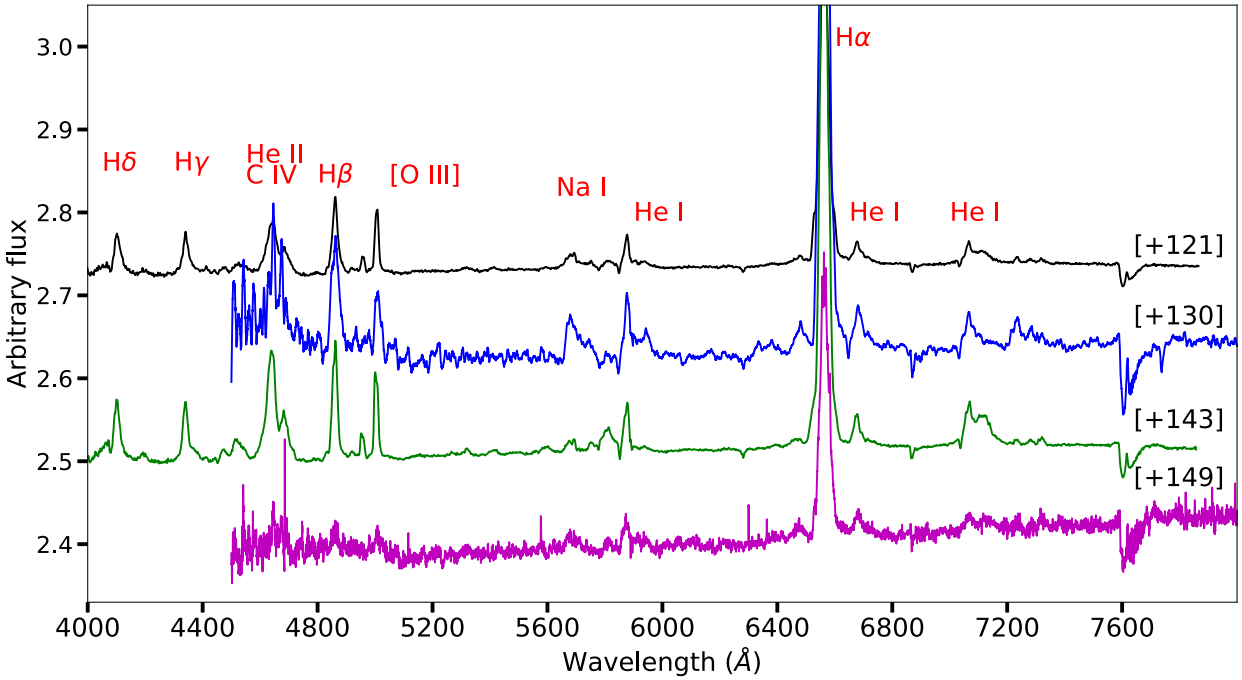

Figure A2. Optical spectral evolution of V1047 Cen. The numbers in brackets are days since t_0.

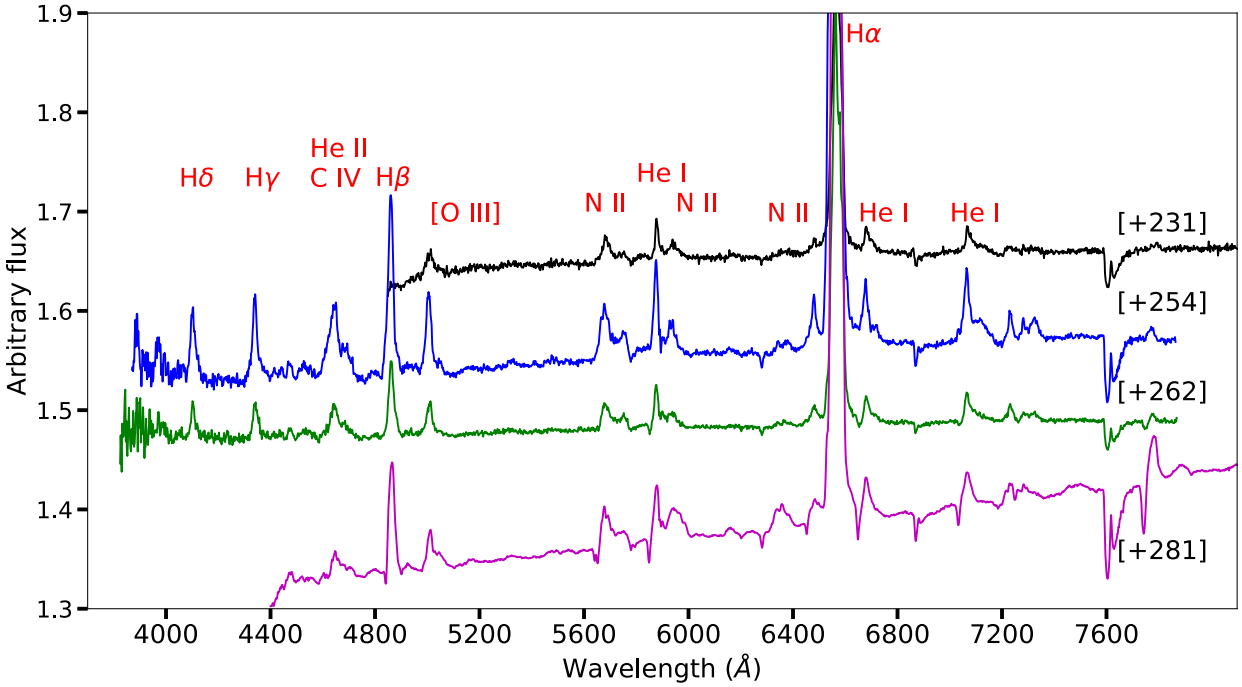

Figure A3. Optical spectral evolution of V1047 Cen. The numbers in brackets are days since t_0.

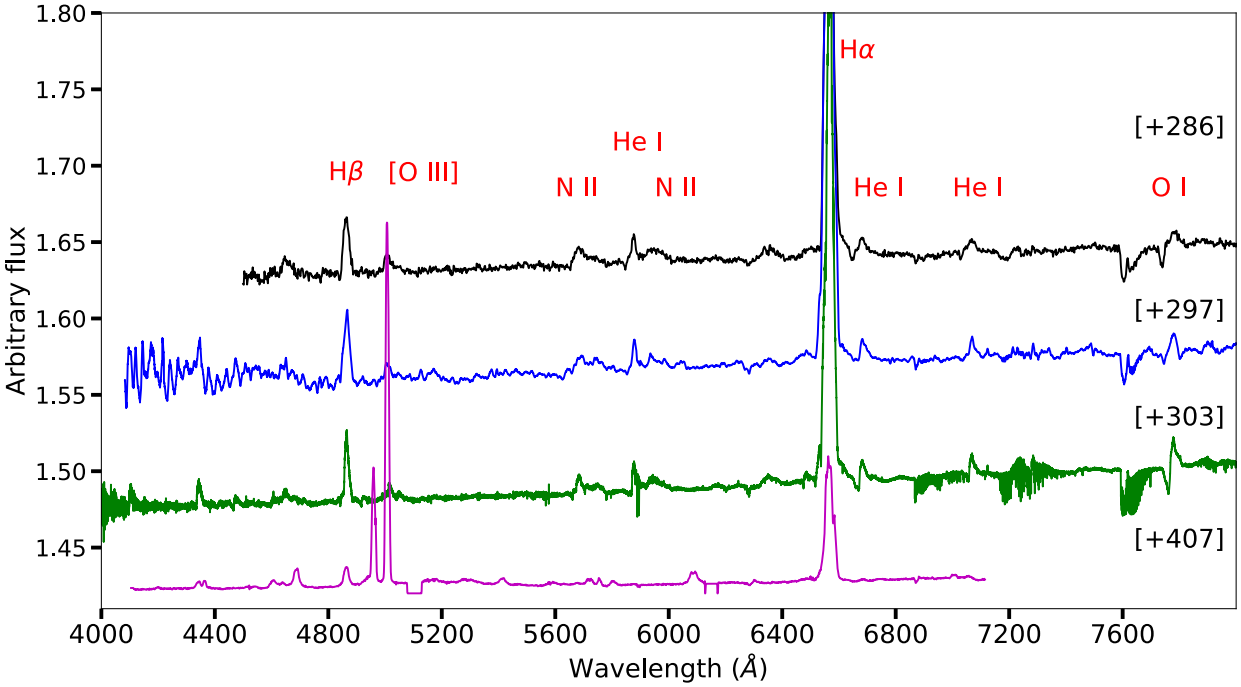

Figure A4. Optical spectral evolution of V1047 Cen. The numbers in brackets are days since t_0.

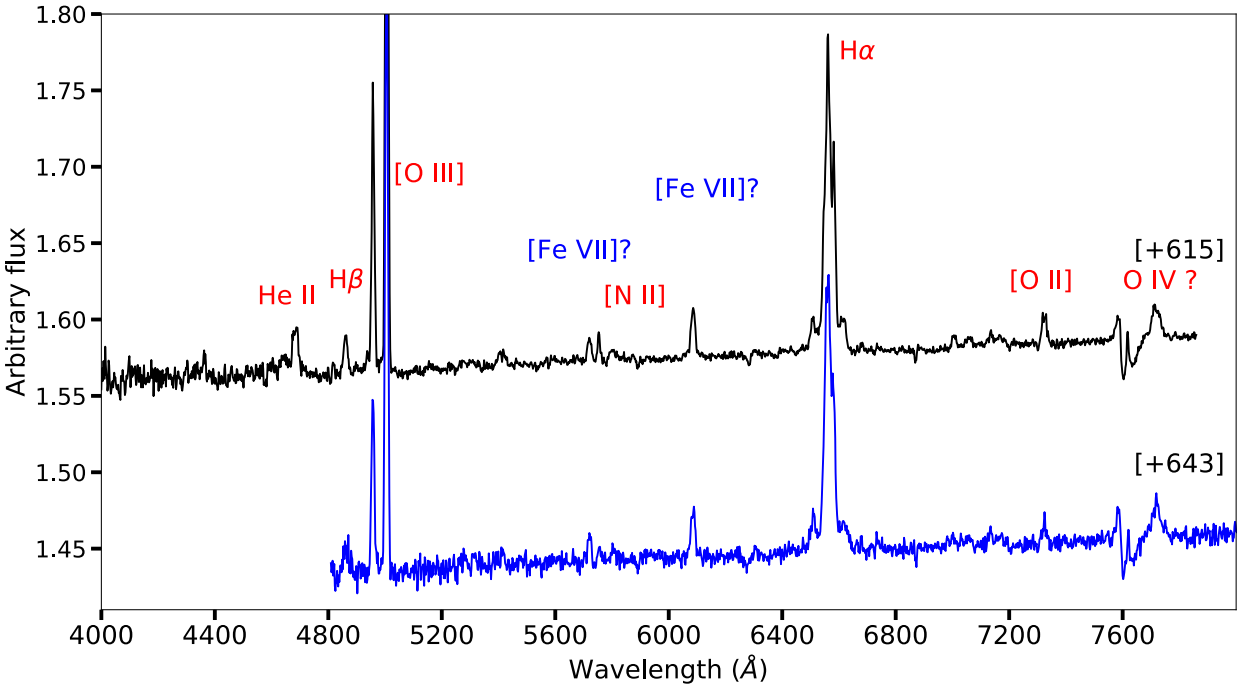

Figure A5. Optical spectral evolution of V1047 Cen. The numbers in brackets are days since t_0.

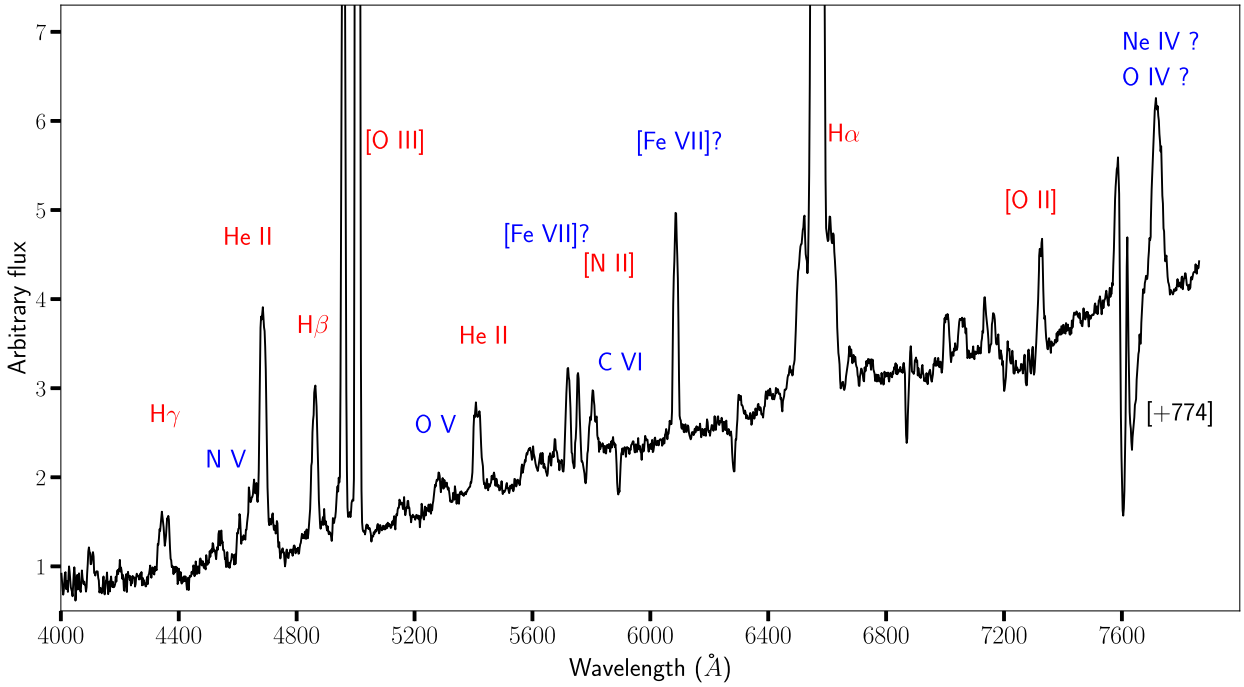

Figure A6. Optical spectral evolution of V1047 Cen. The numbers in brackets are days since t_0.

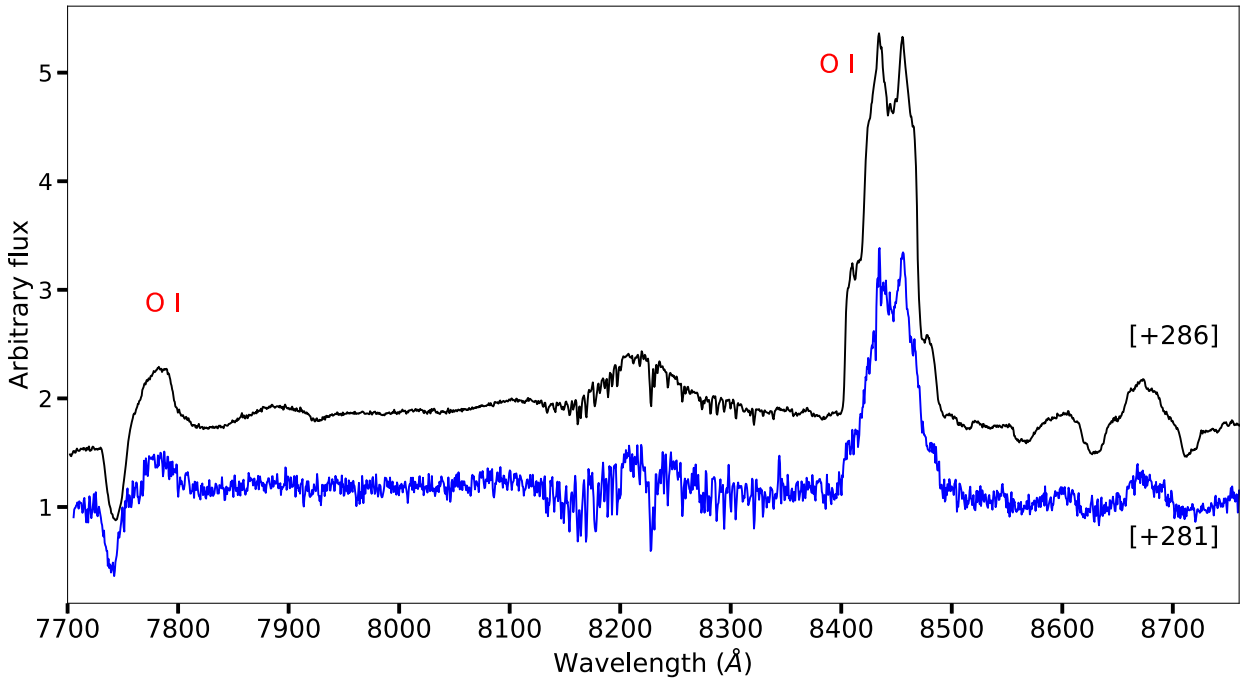

Figure A7. Optical spectral evolution of V1047 Cen. The numbers in brackets are days since t_0.

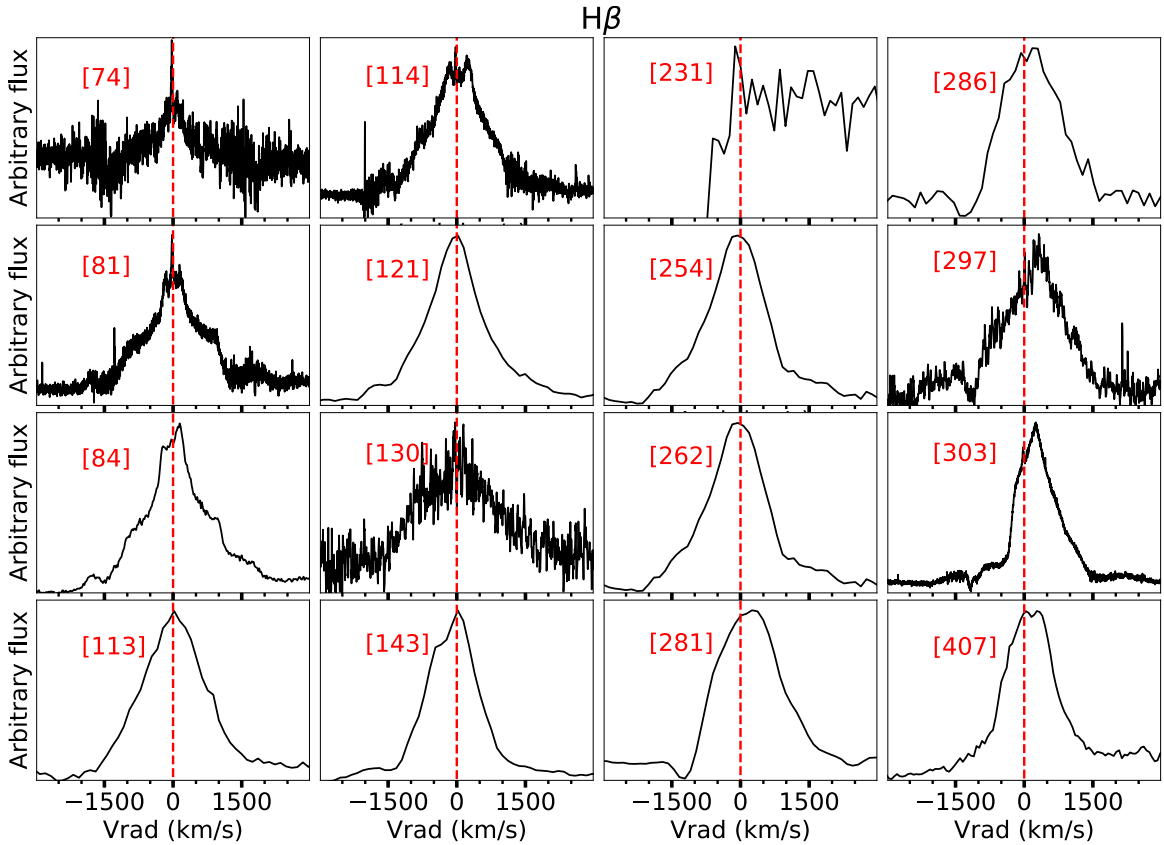

Figure A8. Line profile evolution of Hβ throughout the outburst of V1047 Cen. The numbers between brackets are days after outburst. The red dashed lines represent the rest velocity ($V_{\rm vrad} = 0$ km s^{-1}). A heliocentric correction is applied to the radial velocities.

Table A1
Log of the OGLE Optical Photometry

JD	Magnitude	Err.	Band
2456437.64553	17.190	0.037	*I*
2456438.65480	17.325	0.040	*I*
2456465.62998	17.052	0.028	*I*
2456467.65411	17.075	0.033	*I*
2456478.47615	17.156	0.025	*I*
2456494.56288	17.111	0.043	*I*
2456500.50861	17.094	0.032	*I*
2456522.47809	17.061	0.036	*I*
2456693.83993	16.963	0.017	*I*
2456699.82818	17.020	0.020	*I*
2456702.84838	17.012	0.021	*I*
2456705.81657	16.981	0.027	*I*
2456713.85601	17.076	0.021	*I*

Table A2
Log of the AAVSO Optical Photometry

JD	Magnitude	Err.	Band
2458655.4927	15.488	0.032	*V*
2458655.4938	15.503	0.026	*V*
2458655.4947	13.807	0.033	*I*
2458655.4954	13.846	0.038	*I*
2458655.4962	14.672	0.029	*R*
2458655.4970	14.636	0.030	*R*
2458656.4909	15.472	0.049	*V*
2458656.4911	16.674	0.065	*B*
2458656.4920	15.475	0.036	*V*
2458656.4929	13.718	0.051	*I*
2458656.4936	13.709	0.040	*I*
2458656.4945	14.542	0.032	*R*
2458656.4952	14.531	0.030	*R*
2458656.4963	16.497	0.056	*B*
2458656.4977	16.468	0.058	*B*

Table A3
Log of the SMARTS NIR Photometry

JD	Magnitude	Err.	Band
2458656.49902	12.265	0.016	*H*
2458656.50000	11.864	0.018	*K*
2458656.50000	13.014	0.025	*J*
2458657.51172	11.465	0.019	*K*
2458657.51172	11.967	0.013	*H*
2458657.51172	12.682	0.027	*J*
2458657.51562	12.057	0.012	*H*
2458657.51660	11.602	0.018	*K*
2458657.51660	12.735	0.025	*J*
2458660.50195	11.327	0.018	*K*

Table A4
Log of the NEOWISE NIR Photometry

JD	Magnitude	Err.	Band
2458685.13	9.224	0.092	*W1*
2458685.13	8.382	0.083	*W2*
2458887.15	8.368	0.083	*W1*
2458887.15	7.741	0.074	*W2*
2458894.82	8.585	0.085	*W1*
2458894.82	7.998	0.079	*W2*
2459049.28	12.119	0.121	*W1*
2459049.28	10.737	0.107	*W2*

Table A5
Optical Spectroscopic Observation Log

Telescope	Instrument	Date	$t - t_0$ (days)	Resolving Power	λ Range (Å)
SALT	HRS	2019-6-19	74	14,000	4000–9000
SALT	HRS	2019-6-26	81	14,000	4000–9000
SOAR	Goodman	2019-6-29	84	5000	4500–5170
SOAR	Goodman	2019-6-29	84	5000	6130–6710
SMARTS	CHIRON	2019-7-17	104	28,000	4080–8900
SOAR	Goodman	2019-7-28	113	1000	3800–7800
SOAR	Goodman	2019-7-28	113	5000	6130–6710
SALT	HRS	2019-7-29	114	14,000	4000–9000
SOAR	Goodman	2019-8-5	121	1000	3800–7800
SOAR	Goodman	2019-8-5	121	5000	6130–6710
SMARTS	CHIRON	2019-8-14	130	28,000	4080–8900
SOAR	Goodman	2019-8-27	143	1000	3800–7800
SOAR	Goodman	2019-8-27	143	5000	6130–6710
SMARTS	CHIRON	2019-9-2	149	28,000	4080–8900
SOAR	Goodman	2019-11-23	231	1000	3800–7800
SOAR	Goodman	2019-11-23	231	5000	6130–6710
SOAR	Goodman	2019-12-16	254	1000	3800–7800
SOAR	Goodman	2019-12-16	254	5000	6130–6710
SOAR	Goodman	2019-12-24	262	1000	3800–7800
SOAR	Goodman	2019-12-24	262	5000	6130–6710
SOAR	Goodman	2020-1-12	281	1000	3800–7800
SOAR	Goodman	2020-1-12	281	2800	7700–8870
SOAR	Goodman	2020-1-12	281	5000	6130–6710
SOAR	Goodman	2020-1-17	286	1000	3800–7800
SOAR	Goodman	2020-1-17	286	2800	7700–8870
SOAR	Goodman	2020-1-17	286	5000	6130–6710
SMARTS	CHIRON	2020-1-28	297	28,000	4080–8900
SALT	HRS	2020-2-3	303	14,000	4000–9000
SALT	RSS	2020-5-17	407	1500	4100–7200
SOAR	Goodman	2020-11-12	615	1000	3800–7800
SOAR	Goodman	2021-1-8	643	1000	3800–7800

Table A6
Gemini South/FLAMINGOS-2 Observations of V1047 Cen

Date	$t - t_0$ (days)	Wavelength (μm)	$R_{\max}$ $\lambda/\Delta\lambda$	Integration (s)	Airmass (mean)	Standard Star
2020-2-23	323	1.17–1.30	3000	1200	1.64	(a)
2020-2-23	323	1.49–1.78	3000	1200	1.52	HIP63036
2020-2-23	323	1.95–2.45	3000	1200	1.42	HIP63036
2020-3-1	330	0.89–1.75	1200	120	1.63	HIP63036

Note.
[a] Spectra of HIP63036 and HIP67360 combined to match the airmass of V1047 Cen.

Table A7
Log of MeerKAT Radio Observations at 1.28 GHz

Date	MJD	$(t - t_0)$ (days)	Peak Flux (mJy beam^{-1})	Int. Flux[a] (mJy)	α
2019-11-26	58813.18	234.07	0.93 ± 0.06	0.95 ± 0.08	0.1 ± 0.1
2019-12-15	58832.40	253.29	0.88 ± 0.06	0.92 ± 0.08	0.0 ± 0.1
2019-12-20	58837.44	258.33	0.89 ± 0.07	0.9 ± 0.1	0.5 ± 0.2
2019-12-28	58845.28	266.17	0.93 ± 0.06	0.90 ± 0.08	1.0 ± 0.2
2020-1-3	58851.41	272.30	0.81 ± 0.05	0.88 ± 0.08	...
2020-1-10	58858.42	279.31	0.78 ± 0.05	0.89 ± 0.08	0.8 ± 0.5
2020-1-20	58868.21	289.10	0.87 ± 0.06	0.78 ± 0.07	0.2 ± 0.3
2020-1-25	58873.18	294.07	0.80 ± 0.04	0.91 ± 0.06	0.2 ± 0.2
2020-2-1	58880.29	301.18	0.89 ± 0.05	0.86 ± 0.07	...
2020-2-8	58887.20	308.09	0.84 ± 0.05	0.82 ± 0.07	0.6 ± 0.3
2020-2-15	58894.16	315.05	0.76 ± 0.05	0.83 ± 0.07	0.1 ± 0.2
2020-2-21	58900.25	321.14	0.81 ± 0.05	0.79 ± 0.08	1.5 ± 0.2
2020-3-2	58910.16	331.05	0.75 ± 0.04	0.93 ± 0.06	-0.2 ± 0.2
2021-3-6	59279.20	700.09	0.91 ± 0.05	0.91 ± 0.07	-0.09 ± 0.1

Note.
[a] Integrated flux at 1.28 GHz, calculated by fitting a Gaussian to V1047 Cen and integrating the Gaussian's flux. Spectral indices were derived by imaging in eight frequency channels, fitting a point source in each sub-band image, and fitting the resulting fluxes with a power law. We assume a 10% flux calibration error for the flux in each sub-band, while a 5% flux calibration error is assumed for the full band flux measurement.

Table A8
Log of the Swift UVOT Photometry

JD	Magnitude	Err.	Band
2458659.1322	17.533	0.084	*uvw1*
2458688.9402	17.525	0.080	*uvw1*
2458703.2580	16.927	0.068	*uvw1*
2458659.1284	19.492	0.281	*uvm2*
2458703.2548	18.816	0.188	*uvm2*
2458709.9321	18.564	0.159	*uvm2*
2458718.3840	18.099	0.179	*uvw2*
2458722.2083	18.415	0.122	*uvw2*
2458731.7276	18.178	0.126	*uvw2*

Table A9
Classical and DNe in the Same System

Name	RAJ2000 hh:mm:ss.s	DECJ2000	CN Epoch/ Date	CN Peak mag	DN Epoch Date	DN Peak mag
GK Per	03:31:12.01	+43°54′15.5″	2415439/1901-2-23	$V = 0.2$	1981	10.2
V392 Per	04:43:21.37	+47°21′25.9″	2458238/2018-4-29	$V = 6.3$	1999–2004	13
GI Mon	07:26:47.11	−06°40′29.7″	1918	$V = 5.2$		
AT Cnc	08:28:36.93	+25°20′03.0″	1645	?	2005	12.5
V1213 Cen	13:31:15.81	−63°57′38.0″	2009-5-8	$V = 8.5$	2003	$I = 19.5$
X Ser	16:19:17.69	−02°29′29.5″	1903-3-26	8.9	2016-9-3	14
Nova Sco 1437	17:01:28.15	−43°06′12.3″	1437	?	2017-5-27	$V = 13.2$
V2109 Oph	17:24:16.04	−24°36′50.0″	1969-6-8	$B = 8.9$	2021-8-24	$G = 16.5$
V908 Oph	17:28:04.58	−27°43′04.4″	2434925/1954-7-1	<9	OGLE-IV > 2010	$I = 18.2$
V728 Sco	17:39:13.24	−45°28′45.7″	1862	$V = 5.0$	2013–2015	$V \approx 17$
V1017 Sgr	18:32:04.47	−29°23′12.6″	1919	$B = 6.4$	1973	10.5
V446 Her	18:57:21.60	+13°14′29.0″	1960-3-3	2.8	1994	15.8
V606 Aql	19:20:24.29	−00°08′07.8″	1899-4-21	5.5	2019-10-20	$g = 19$
WY Sge	19:32:43.87	+17°44′54.5″	1783	5.4	1982-6-17	17.7
V476 Cyg	19:58:24.46	+53°37′07.5″	1920	2.0	2019-8-24	$g \approx 16.5$

Note. GK Per: Sabbadin & Bianchini (1983); Zemko et al. (2017); Williams & Darnley (2018), V392 Per: Liu & Hu (2000); Munari et al. (2020); Murphy-Glaysher et al. (2022), AT Cnc: Shara et al. (2012), V1017 Sgr: Salazar et al. (2017), V908 Oph: Tappert et al. (2016); Mróz et al. (2015), V606 Aql: Tappert et al. (2016); Duerbeck (1987); Bellm et al. (2019), WY Sge: Shara et al. (1984), X Ser: Payne-Gaposchkin (1957), V446 Her: Cragg (1960), Nova Sco 1437: Kochanek et al. (2017); Shara et al. (2017) V1213 Cen: Mróz et al. (2016), V728 Sco: Vogt et al. (2018); Kato (2022), V476 Cyg: Kato (2022). For systems with multiple DN outbursts, we list the brightest detected outburst found from a literature search. The objects in this table were found by searching the AAVSO Variable Star Index (VSX) for variability types containing a classical nova plus a DN identifier. It is possible that this list is not complete.

ORCID iDs

E. Aydi https://orcid.org/0000-0001-8525-3442
K. V. Sokolovsky https://orcid.org/0000-0001-5991-6863
E. Tremou https://orcid.org/0000-0002-4039-6703
A. Evans https://orcid.org/0000-0002-3142-8953
J. Strader https://orcid.org/0000-0002-1468-9668
L. Chomiuk https://orcid.org/0000-0002-8400-3705
G. Myers https://orcid.org/0000-0002-9810-0506
F-J. Hambsch https://orcid.org/0000-0003-0125-8700
K. L. Page https://orcid.org/0000-0001-5624-2613
C. E. Woodward https://orcid.org/0000-0001-6567-627X
F. M. Walter https://orcid.org/0000-0001-7796-1756
P. Mróz https://orcid.org/0000-0001-7016-1692
T. R. Geballe https://orcid.org/0000-0003-2824-3875
D. P. K. Banerjee https://orcid.org/0000-0003-4896-2543
R. D. Gehrz https://orcid.org/0000-0003-1319-4089
M. Gromadzki https://orcid.org/0000-0002-1650-1518
A. Kawash https://orcid.org/0000-0003-0071-1622
K. Mukai https://orcid.org/0000-0002-8286-8094
U. Munari https://orcid.org/0000-0001-6805-9664
M. Orio https://orcid.org/0000-0003-1563-9803
V. A. R. M. Ribeiro https://orcid.org/0000-0003-3617-4400
S. Starrfield https://orcid.org/0000-0002-1359-6312
A. Udalski https://orcid.org/0000-0001-5207-5619
P. A. Woudt https://orcid.org/0000-0002-6896-1655

References

Aydi, E., Buckley, H. D. A., Mroz, P., et al. 2019a, ATel, 12885, 1
Aydi, E., Sokolovsky, K., Chomiuk, L., et al. 2019b, ATel, 12889, 1
Bahramian, A., Heinke, C. O., Degenaar, N., et al. 2015, MNRAS, 452, 3475
Bahramian, A., Miller-Jones, J., Strader, J., et al. 2018, Radio/X-ray correlation database for X-ray binaries, v0.1, Zenodo, doi:10.5281/zenodo.1252036
Ballester, P 1992, in European Southern Observatory Conf. and Workshop Proc., 41, European Southern Observatory Conf. and Workshop Proc., ed. P. J. Grosbøl & R. C. E. de Ruijsscher (Garching: ESO), 177
Barnes, S. I., Cottrell, P. L., Albrow, M. D., et al. 2008, Proc. SPIE, 7014, 70140K
Barrett, P., Dieck, C., Beasley, A. J., Mason, P. A., & Singh, K. P. 2020, AdSpR, 66, 1226
Barrett, P. E., Dieck, C., Beasley, A. J., Singh, K. P., & Mason, P. A. 2017, AJ, 154, 252
Bellm, E. C., Kulkarni, S. R., Graham, M. J., et al. 2019, PASP, 131, 018002
Bianchini, A., Sabbadin, F., Favero, G. C., & Dalmeri, I. 1986, A&A, 160, 367
Bode, M. F., & Evans, A. 2008, Classical Novae (Cambridge: Cambridge Univ. Press)
Bode, M. F., Seaquist, E. R., & Evans, A. 1987, MNRAS, 228, 217
Bollimpalli, D. A., Hameury, J. M., & Lasota, J. P. 2018, MNRAS, 481, 5422
Bramall, D. G., Sharples, R., Tyas, L., et al. 2010, Proc. SPIE, 7735, 77354F
Bramall, D. G., Schmoll, J., Tyas, L. M. G., et al. 2012, Proc. SPIE, 8446, 84460A
Brocksopp, C., Sokoloski, J. L., Kaiser, C., et al. 2004, MNRAS, 347, 430
Buckley, D. A. H., Swart, G. P., & Meiring, J. G. 2006, Proc. SPIE, 6267, 62670Z
Burgh, E. B., Nordsieck, K. H., Kobulnicky, H. A., et al. 2003, Proc. SPIE, 4841, 1463
Burmeister, M., & Leedjärv, L. 2007, A&A, 461, L5
Burrows, D. N., Hill, J. E., Nousek, J. A., et al. 2005, SSRv, 120, 165
Carey, S. J., Noriega-Crespo, A., Mizuno, D. R., et al. 2009, PASP, 121, 76
Chen, B. Q., Huang, Y., Yuan, H. B., et al. 2019, MNRAS, 483, 4277
Chomiuk, L., Metzger, B. D., & Shen, K. J. 2021a, ARA&A, 59, 391
Chomiuk, L., Linford, J. D., Aydi, E., et al. 2021b, ApJS, 257, 49
Cieslinski, D., Diaz, M. P., & Steiner, J. E. 1999, AJ, 117, 534
Clarke, M., Vacca, W. D., & Shuping, R. Y. 2015, in ASP Conf. Ser., 495, Redux: A Common Interface for SOFIA Data Reduction Pipelines, ed. A. R. Taylor & E. Rosolowsky (San Francisco, CA: ASP), 355
Clayton, D. D. 1968, Principles of Stellar Evolution and Nucleosynthesis (Chicago, IL: Univ. Chicago Press)
Clemens, J. C., Crain, J. A., & Anderson, R. 2004, Proc. SPIE, 5492, 331
Coppejans, D. L., & Knigge, C. 2020, NewAR, 89, 101540
Coppejans, D. L., Körding, E. G., Miller-Jones, J. C. A., et al. 2015, MNRAS, 451, 3801
Coppejans, D. L., Körding, E. G., Miller-Jones, J. C. A., et al. 2016, MNRAS, 463, 2229
Córdova, F. A., Mason, K. O., & Hjellming, R. M. 1983, PASP, 95, 69
Cragg, T. A. 1960, PASP, 72, 475
Crause, L. A., Sharples, R. M., Bramall, D. G., et al. 2014, Proc. SPIE, 9147, 91476T
Crawford, S. M., Still, M., Schellart, P., et al. 2010, Proc. SPIE, 7737, 25
Crocker, M. M., Davis, R. J., Eyres, S. P. S., et al. 2001, MNRAS, 326, 781

Darnley, M. J., Ribeiro, V. A. R. M., Bode, M. F., Hounsell, R. A., & Williams, R. P. 2012, ApJ, 746, 61
Delgado, A., Harrison, D., Hodgkin, S., et al. 2019, TNSTR, 2019, 1
Della Valle, M., & Izzo, L. 2020, A&ARv, 28, 3
Duerbeck, H. W. 1987, SSRv, 45, 1
Evans, A., & Gehrz, R. D. 2012, BASI, 40, 213
Evans, P. A., Beardmore, A. P., Osborne, J. P., & Wynn, G. A. 2009, MNRAS, 399, 1167
Feinstein, A. D., Montet, B. T., Foreman-Mackey, D., et al. 2019, PASP, 131, 094502
Friedman, S. D., York, D. G., McCall, B. J., et al. 2011, ApJ, 727, 33
Fujimoto, M. Y. 1982, ApJ, 257, 752
Gaia Collaboration, Brown, A. G. A., Vallenari, A., et al. 2021, A&A, 649, A1
Gallagher, J. S., & Starrfield, S. 1976, MNRAS, 176, 53
Gallagher, J. S., & Starrfield, S. 1978, ARA&A, 16, 171
Geballe, T. R., Banerjee, D. P. K., Evans, A., et al. 2019, ApJL, 886, L14
Gehrels, N., Chincarini, G., Giommi, P., et al. 2004, ApJ, 611, 1005
Gehrz, R. D., Evans, A., Helton, L. A., et al. 2015, ApJ, 812, 132
Ginzburg, S., & Quataert, E. 2021, MNRAS, 507, 475
Gordon, A. C., Aydi, E., Page, K. L., et al. 2021, ApJ, 910, 134
Gutermuth, R. A., & Heyer, M. 2015, AJ, 149, 64
Hachisu, I., & Kato, M. 2007, ApJ, 662, 552
Helton, L. A., Gehrz, R. D., Woodward, C. E., et al. 2012, ApJ, 755, 37
Herbig, G. H., Preston, G. W., Smak, J., & Paczynski, B. 1965, ApJ, 141, 617
Herter, T. L., Adams, J. D., Gull, G. E., et al. 2018, JAI, 7, 1840005
Heywood, I. 2020, OxKAT: Semi-automated Imaging of MeerKAT Observations, Astrophysics Source Code Library, ascl:2009.003
Hillman, Y., Orio, M., Prialnik, D., et al. 2019, ApJL, 879, L5
Hillman, Y., Shara, M. M., Prialnik, D., & Kovetz, A. 2020, NatAs, 4, 886
Honeycutt, R. K., Robertson, J. W., & Kafka, S. 2011, AJ, 141, 121
Honeycutt, R. K., Robertson, J. W., & Turner, G. W. 1995, ApJ, 446, 838
Jonas, J. & MeerKAT Team 2016, in Proceedings of MeerKAT Science: On the Pathway to the SKA (Trieste: PoS)
Kafka, S. 2020, EPSC, 14, EPSC2020-314
Kato, T. 2022, arXiv:2203.06320
Kawash, A., Chomiuk, L., Strader, J., et al. 2021, ApJ, 910, 120
Kniazev, A. Y., Gvaramadze, V. V., & Berdnikov, L. N. 2016, MNRAS, 459, 3068
Kobulnicky, H. A., Nordsieck, K. H., Burgh, E. B., et al. 2003, Proc. SPIE, 4841, 1634
Kochanek, C. S., Shappee, B. J., Stanek, K. Z., et al. 2017, PASP, 129, 104502
Körding, E., Rupen, M., Knigge, C., et al. 2008, Sci, 320, 1318
Kovetz, A., & Prialnik, D. 1985, ApJ, 291, 812
Liller, W., Jacques, C., Pimentel, E., Aguiar, J. G. D. S., & Shida, R. Y. 2005, IAU Circ., 8596, 1
Liu, W., & Hu, J. Y. 2000, ApJS, 128, 387
Livio, M. 1992, ApJ, 393, 516
MacDonald, J. 1996, in Astrophysics and Space Science Library, Vol. 208, IAU Colloq. 158: Cataclysmic Variables and Related Objects, ed. A. Evans & J. H. Wood (Kluwer: Dordrecht), 281
Mainzer, A., Bauer, J., Grav, T., et al. 2011, ApJ, 731, 53
Mikołajewska, J. 2002, MNRAS, 335, L33
Mikołajewska, J. 2003, in ASP Conf. Ser., 303, Symbiotic Stars Probing Stellar Evolution, ed. R. L. M. Corradi, J. Mikolajewska, & T. J. Mahoney (San Francisco, CA: ASP), 9
Mikołajewska, J. 2012, BaltA, 21, 5
Miller-Jones, J. C. A., Sivakoff, G. R., Knigge, C., et al. 2013, Sci, 340, 950
Miller-Jones, J. C. A., Sivakoff, G. R., Altamirano, D., et al. 2011, Jets at All Scales, 275 ed. G. E. Romero, R. A. Sunyaev, & T. Belloni, 224
Mohamed, S., & Podsiadlowski, P. 2007, in ASP Conf. Ser., 372, 15th European Workshop on White Dwarfs, ed. R. Napiwotzki & M. R. Burleigh (San Francisco, CA: ASP), 397
Monet, D. G., Levine, S. E., Canzian, B., et al. 2003, AJ, 125, 984
Morales-Rueda, L., & Marsh, T. R. 2002, MNRAS, 332, 814
Mroz, P., & Udalski, A. 2019, ATel, 12876, 1
Mróz, P., Udalski, A., Poleski, R., et al. 2015, ApJS, 219, 26
Mróz, P., Udalski, A., Pietrukowicz, P., et al. 2016, Natur, 537, 649
Mukai, K., Orio, M., & Della Valle, M. 2008, ApJ, 677, 1248
Munari, U. 2019, arXiv:1909.01389
Munari, U., Moretti, S., & Maitan, A. 2020, A&A, 639, L10
Munari, U., Siviero, A., & Henden, A. 2005, MNRAS, 360, 1257
Murphy-Glaysher, F. J., Darnley, M. J., Harvey, É. J., et al. 2022, MNRAS, 514, 6183
Ness, J. U., Schwarz, G. J., Retter, A., et al. 2007, ApJ, 663, 505
O'Donoghue, D., Buckley, D. A. H., Balona, L. A., et al. 2006, MNRAS, 372, 151
Ogley, R. N., Chaty, S., Crocker, M., et al. 2002, MNRAS, 330, 772
Page, K. L., Beardmore, A. P., & Osborne, J. P. 2020, AdSpR, 66, 1169
Payne-Gaposchkin, C. H. P. 1957, in The Galactic Novae, ed. I. P. Amsterdam (New York: North-Holland Pub. Co.)
Ramsay, G., Schreiber, M. R., Gänsicke, B. T., & Wheatley, P. J. 2017, A&A, 604, A107
Ricker, G. R., Winn, J. N., Vanderspek, R., et al. 2015, JATIS, 1, 014003
Roming, P. W. A., Kennedy, T. E., Mason, K. O., et al. 2005, SSRv, 120, 95
Russell, T. D., Miller-Jones, J. C. A., Sivakoff, G. R., et al. 2016, MNRAS, 460, 3720
Sabbadin, F., & Bianchini, A. 1983, A&AS, 54, 393
Saito, R. K., Hempel, M., Minniti, D., et al. 2012, A&A, 537, A107
Salazar, I. V., LeBleu, A., Schaefer, B. E., Landolt, A. U., & Dvorak, S. 2017, MNRAS, 469, 4116
Schaefer, B. E. 2010, ApJS, 187, 275
Schaefer, B. E., & Collazzi, A. C. 2010, AJ, 139, 1831
Schlafly, E. F., & Finkbeiner, D. P. 2011, ApJ, 737, 103
Schwarz, G. J., Ness, J.-U., Osborne, J. P., et al. 2011, ApJS, 197, 31
Seaquist, E. R., & Taylor, A. R. 1990, ApJ, 349, 313
Seaquist, E. R., Taylor, A. R., & Button, S. 1984, ApJ, 284, 202
Sekiguchi, K. 1992, Natur, 358, 563
Shafter, A. W., Darnley, M. J., Hornoch, K., et al. 2011, ApJ, 734, 12
Shara, M. M., Livio, M., Moffat, A. F. J., & Orio, M. 1986, ApJ, 311, 163
Shara, M. M., Mizusawa, T., Wehinger, P., et al. 2012, ApJ, 758, 121
Shara, M. M., Moffat, A. F. J., McGraw, J. T., et al. 1984, ApJ, 282, 763
Shara, M. M., Prialnik, D., & Shaviv, G. 1977, A&A, 61, 363
Shara, M. M., Iłkiewicz, K., Mikołajewska, J., et al. 2017, Natur, 548, 558
Shara, M. M., Doyle, T. F., Pagnotta, A., et al. 2018, MNRAS, 474, 1746
Shortridge, K., Meyerdierks, H., & Bridger, A. 1992, Figaro Release Notes–Standard and National Figaro 3.0-3, Starlink System Note, 40
Skopal, A., Tomov, N. A., & Tomova, M. T. 2013, A&A, 551, L10
Sokoloski, J. L., Kenyon, S. J., Espey, B. R., et al. 2006, ApJ, 636, 1002
Stahl, O., Kaufer, A., & Tubbesing, S. 1999, in ASP Conf. Ser., 188, Optical and Infrared Spectroscopy of Circumstellar Matter, ed. E. Guenther, B. Stecklum, & S. Klose (San Francisco, CA: ASP), 331
Starrfield, S., Bose, M., Iliadis, C., et al. 2020, ApJ, 895, 70
Starrfield, S., Iliadis, C., & Hix, W. R. 2008, in Classical Novae, (Cambridge Astrophysics Series), ed. M. F. Bode & A. Evans, Vol. 43 (2nd ed.; Cambridge: Cambridge Univ. Press), 77
Starrfield, S., Timmes, F. X., Hix, W. R., et al. 2004, ApJL, 612, L53
Starrfield, S., Truran, J. W., Sparks, W. M., & Kutter, G. S. 1972, ApJ, 176, 169
Steiner, J. E., Cieslinski, D., Jablonski, F. J., & Williams, R. E. 1999, A&A, 351, 1021
Strope, R. J., Schaefer, B. E., & Henden, A. A. 2010, AJ, 140, 34
Tappert, C., Barria, D., Fuentes Morales, I., et al. 2016, MNRAS, 462, 1371
Tody, D. 1986, Proc. SPIE, 627, 733
Tody, D. 1993, in ASP Conf. Ser., 52, Astronomical Data Analysis Software and Systems II, ed. R. J. Hanisch, R. J. V. Brissenden, & J. Barnes (San Francisco, CA: ASP), 173
Tokovinin, A., Fischer, D. A., Bonati, M., et al. 2013, PASP, 125, 1336
Tomov, N., & Tomova, M. 2013, IBVS, 6055, 1
Udalski, A., Szymański, M. K., & Szymański, G. 2015, AcA, 65, 1
Vogt, N., Tappert, C., Puebla, E. C., et al. 2018, MNRAS, 478, 5427
Walter, F. M., Battisti, A., Towers, S. E., Bond, H. E., & Stringfellow, G. S. 2012, PASP, 124, 1057
Wang, S., & Chen, X. 2019, ApJ, 877, 116
Warner, B. 1995, Cataclysmic Variable Stars, Vol. 28 (Cambridge: Cambridge Univ. Press)
Wilber, A., Neric, M., Starrfield, S., Wagner, R. M., & Woodward, C. E. 2015, ATel, 7217, 1
Williams, S. C., & Darnley, M. J. 2018, ATel, 11995, 1
Wolf, W. M., Bildsten, L., Brooks, J., & Paxton, B. 2013, ApJ, 777, 136
Woudt, P. A., & Ribiero, V. A. R. M. 2014, in ASP Conf. Ser., 490, Stella Novae: Past and Future Decades (San Francisco, CA: ASP)
Yaron, O., Prialnik, D., Shara, M. M., & Kovetz, A. 2005, ApJ, 623, 398
Young, E. T., Becklin, E. E., Marcum, P. M., et al. 2012, ApJL, 749, L17
Zemko, P., Mukai, K., & Orio, M. 2015, ApJ, 807, 61
Zemko, P., Orio, M., Luna, G. J. M., et al. 2017, MNRAS, 469, 476
Zemko, P., Orio, M., Mukai, K., et al. 2016, MNRAS, 460, 2744